Distribution
Category UC-94E

SAND 83-2343
Unlimited Release
Printed November 1984

LONG-TERM PERFORMANCE PREDICTIONS FOR STRATEGIC PETROLEUM RESERVE (SPR) SALT CAVERNS

Dale S. Preece
Jerry T. Foley
Sandia National Laboratories
Albuquerque, New Mexico 87185

ABSTRACT

A finite element computer program was used to predict creep closure of oil storage caverns in two salt domes in the Gulf Coast region of the United States. These caverns are part of the U.S. Strategic Petroleum Reserve (SPR) Program which is administered by the U.S. Department of Energy (DOE).

The resulting stresses and displacements predicted by the finite element program were post-processed to obtain: 1) a measure of the structural integrity of each cavern and 2) predictions of well head pressure increase and volume change due to creep closure.

The caverns were determined to be structurally stable through the use of a fracture function which is dependent on mean stress and creep strain. The finite element predictions of pressure increase and volume change were compared to field measurements from caverns presently in use. Finite element predictions were found to be below available measured field data. This IS partially due to the fact that the field data includes the pressure increase from fluid thermal expansion as well as that from creep closure.

*This work was performed at Sandia National Laboratories and was supported by the U.S. Department of Energy under contract number DE-AC04-76DP00789.

TABLE OF CONTENTS

	Page
List of Tables	7
List of Figures	8
1. INTRODUCTION	11
2. ANALYSIS METHODS	11
2.1 Finite Element Analysis	11
2.2 Determining Model Width	12
2.3 Determining Model Height	13
2.4 Boundary Conditions	13
2.5 Simulating Initial Cavern Leaching	14
2.6 Simulating Cavern Leaching During Oil Withdrawal	15
2.7 Temperature Effects	15
2.8 Material Properties	16
2.9 Predicting Salt Fracture	17
2.10 Volumetric Calculations	18
2.11 Analysis of Newly Leached Expansion Caverns	19
3. BRYAN MOUND SALT DOME ANALYSIS RESULTS	20
3.1 General Site Description	20
3.2 Bryan Mound Cavern One	20
3.3 Bryan Mound Cavern Two	21
3.4 Bryan Mound Cavern Three	22
3.5 Bryan Mound Cavern Four	23
3.6 Bryan Mound Cavern Five	24
3.7 Bryan Mound Expansion Caverns	25
4. WEST HACKBERRY SALT DOME ANALYSIS RESULTS	26
4.1 General Site Description	26

4.2 West Hackberry Cavern Six 27

4.3 West Hackberry Cavern Seven 28

4.4 West Hackberry Cavern Eight 29

4.5 West Hackberry Cavern Nine 30

4.6 West Hackberry Cavern Eleven 31

4.7 West Hackberry Expansion Caverns 32

5. COMPARISON WITH FIELD DATA 33

6. CONCLUSIONS 34

7. ACKNOWLEDGEMENTS 35

8. REFERENCES 36

LIST OF TABLES

		Page
TABLE I:	Material Properties	17
TABLE I I:	Bryan Mound Cavern One Predicted Cavern Closure Rates	21
TABLE I I I:	Bryan Mound Cavern Two Predicted Cavern Closure Rates	22
TABLE IV:	Bryan Mound Cavern Four Predicted Cavern Closure Rates	24
TABLE V:	Bryan Mound Cavern Five Predicted Cavern Closure Rates	25
TABLE VI:	Bryan Mound Expansion Cavern Predicted Cavern Closure Rates	26
TABLE VI I:	West Hackberry Cavern Six Predicted Cavern Closure Rates	28
TABLE VIII:	West Hackberry Cavern Seven Predicted Cavern Closure Rates	29
TABLE IX:	West Hackberry Cavern Eight Predicted Cavern Closure Rates	30
TABLE X:	West Hackberry Cavern Nine Predicted Cavern Closure Rates	31
TABLE XI:	West Hackberry Cavern Eleven Predicted Cavern Closure Rates	32
TABLE XII:	West Hackberry Expansion Cavern Predicted Cavern Closure Rates	32
TABLE XIII:	Comparisons of Finite Element Predictions and Field Data	34

LIST OF FIGURES

		Page
Figure 1:	Top View of Cylindrical Cavern Array.....	38
Figure 2:	Axisymmetric Finite Element Model of Cylindrical Cavern.....	39
Figure 3:	Top View of Typical Cavern Group.....	40
Figure 4:	Axisymmetric Finite Element Model of Bryan Mound Cavern One.....	41
Figure 5:	Flowrate Versus Time For Three Different Treatments of the Initial Leaching Process.....	42
Figure 6:	Bryan Mound Cavern One With Leached Layers Crosshatched.....	43
Figure 7:	Volumetric Response of Bryan Mound Cavern One.....	44
Figure 8:	Final Leaching Cycle of Bryan Mound Cavern One.....	45
Figure 9:	Axisymmetric Finite Element Model of Standard Expansion Cavern.....	46
Figure 10:	Axisymmetric Finite Element Model of West Hackberry Salt Dome.....	47
Figure 11:	Vertical Stress In West Hackberry Salt Dome....	48
Figure 12:	Vertical Stress Versus Time 500 Feet Above Toroid B.....	49
Figure 13:	Plan View of Bryan Mound Salt Dome.....	50
Figure 14:	Bryan Mound Cavern One.....	51
Figure 15:	Bryan Mound Cavern Two.....	52
Figure 16:	Axisymmetric Finite Element Model of Bryan Mound Cavern Two.....	53
Figure 17:	Volumetric Response of Bryan Mound Cavern Two.....	54
Figure 18:	Bryan Mound Cavern Three.....	55
Figure 19:	Axisymmetric Finite Element Model of Bryan Mound Cavern Three.....	56

Figure 20. Bryan Mound Cavern Four..... 57

Figure 21. Axisymmetric
58

Figure
59

60

Figure
61

Figure
62

Figure
63

64

65

Axisymmetric
Six..... 66

Figure
67

Figure 68

Figure
69

70

71

Finite
72

Volumetric Response of West Hackberry Cavern Eight..... 73

Figure 37. West Hackberry Cavern Nine..... 74

Figure 38. Close-up of Axisymmetric Finite Element Model of West Hackberry Cavern Nine..... 75

Figure 39: Volumetric Response of West Hackberry Cavern Nine..... 76

Figure 40: West Hackberry Cavern Eleven..... 77

Figure 41 Axisymmetric Finite 78

Figure Volumetric 79

80

1. INTRODUCTION

The U.S. Strategic Petroleum Reserve (SPR) is a national program devoted to reducing the vulnerability of the United States to supply interruptions by foreign oil suppliers. The program calls for storage of approximately 750 million barrels (MMbbl) of crude oil or more. Salt caverns leached in salt domes around the Gulf of Mexico have been determined to be economical sites to store the majority of this petroleum because the caverns are safer and more economical than steel tanks and because the Gulf Coast location allows easy access to the shipping lanes and pipeline networks which already carry much of the flow of foreign oil into the country. Another advantage to the use of salt domes was the availability of an existing mine and numerous caverns which were suitable for purchase and immediate petroleum storage. The final storage volume will thus be split between an existing mine, existing caverns and newly leached expansion caverns in two salt domes around the Gulf.

The purpose of this report is to present cavern structural stability and creep closure predictions obtained from finite element analyses of caverns filled with brine or oil at Bryan Mound, Texas, and at West Hackberry, Louisiana.

2. ANALYSIS METHODS

2.1 Finite Element Analysis

The finite element method offers the capability to model almost any geometric shape and subject the model to a variety of loading conditions. This makes it ideal for analyzing salt caverns which vary greatly in size, shape and average depth.

A considerable amount of development work has been done on a finite element program to predict the creep response of bedded rock salt [4]. This program was one of nine structural computer programs used in the Benchmark II exercise in which a generic drift for nuclear waste isolation in bedded salt was analyzed [6]. The predicted values from the program compared well

with results from the eight other structural codes which were exercised in the benchmark study.

This program was also used to analyze existing caverns which had been capped and instrumented to provide pressure increase data and/or volume change data due to creep closure. The results of these analyses were in agreement with the field data [8]. Subsequent analyses of other caverns including those documented in this report have typically underpredicted the pressure increase data coming from the wellhead. While the reasons for this are not yet fully understood, it is probably due to a combination of fluid thermal expansion, material modeling and boundary conditions.

2.2 Determining Model Width

The code can currently analyze only two-dimensional plane or axisymmetric shapes. Since the caverns are three-dimensional, some approximation is required. In an idealized array of evenly spaced caverns on the same level, where the rows are staggered, each cavern is surrounded by six other caverns which are all equidistant from the central cavern (a hexagonal, close packed array) as shown in Figure 1. An axisymmetric approximation of this cavern array can be made using the finite element model shown in Figure 2 where the mesh width is one-half the center-to-center distance between caverns.

If, however, an example cavern we desire to analyze is surrounded by caverns at the same level distributed as shown in Figure 3. the even spacing of an orderly array is no longer present. The mesh width for analyzing cavern A in Figure 3 is determined by averaging half the pillar widths to surrounding caverns. In cases where there is a 180° arc around a cavern, where no other caverns exist on the same level, we also include in the averaging process the pillar distance required to simulate an infinite boundary. This distance has been determined to be approximately eight times the cavern diameter [7]. Using this information, we can calculate the mesh width required for cavern A in Figure 3 as

$$W = \frac{AB/2+AC/2+AD/2+8d}{4} + d/2 \qquad (1)$$

The outer boundary of the model describing cavern A is shown in Figure 3. Comparison with limited field data has shown the method to be valid. However, more data and subsequent analysis of the data source would be helpful and is being actively pursued.

2.3 Determining Model Height

Initially, the vertical distance between the top and bottom boundaries of the models was made three times the height of the cavern, with the cavern situated in the middle. This was adequate with a long slender cavern, but not for caverns that are shorter and wider. It was determined, therefore, that there should be at least twice the widest radius of the cavern in model height above and below the cavern and preferably three times. This was determined from calculations of the state of effective stress at the top and bottom boundary after 60 years of creep stress relief. It was considered desirable to have the effective stress at the top and bottom of the model less than ten percent of the effective stress at the surface of the cavern walls. This assured minimal interference of the top of the model with cavern response.

2.4 Boundary Conditions

The finite element model of Bryan Mound Cavern One is shown in Figure 4. The boundary conditions applied to this mesh are typical of those applied to the other caverns in this report. Across the top of the mesh is placed a lithostatic pressure corresponding to its depth (1 psi per foot of depth). Inside the cavern is a brinehead pressure from the surface of the ground (0.521 psi per foot of depth). Even though the cavern contains crude oil, the brine string to the surface from the brine buffer at the cavern bottom results in approximately brinehead pressure in the cavern. Since brinehead pressure is less than lithostatic pressure, the cavern walls will creep inward. The right and left sides of the mesh are allowed to move vertically, but they are fixed horizontally as indicated by the vertical

rollers. The bottom of the mesh is allowed to move horizontally, but it is fixed vertically. The initial stress state is set to be lithostatic across the entire mesh so that the creep algorithm wil 1 have a correct stress state from which to begin computations.

2.5 Simulating Initial Cavern Leaching

Each cavern starts as a borehole and gradually enlarges as fresh water 1s pumped in and brine is pumped out. The borehole disturbs the global state of stress away from the hole very little, 1 eaving a state of lithostatic stress throughout the region where the cavern will be leached. The stress at the current cavern surface gradually changes with time from lithostatic to brinehead as the cavern is developed from a borehole to its present state. It has been determined that this leaching process must be simulated in order to accurately predict the cavern response immediately after leaching is completed. One method is to linearly reduce the pressure inside the current cavern geometry from lithostatic to brinehead over a finite period of time. Figure 5 shows the predicted cavern closure rate (measured in volumetric flowrate) for three different treatments of the initial leaching. Curve A shows the instantaneously created cavern response when it is loaded initially with brinehead pressure inside. In this case, the effective stress around the cavern is very large initially and gradually decays due to creep stress relaxation of the rock salt. The dotted line in Curve A at 500 days represents a computational range where numerical oscillation occurs as the system adjusts to the instantaneous loading. The oscillation was determined to be numerical by observing that the occurrence time and period of the oscillation was a function of the computational time step As the time step was shortened the oscillation moved toward zero and didn't last as long. Curves B and C show the cavern response when the pressure inside is reduced from lithostatic to brinehead over 300 days and 1000 days, respectively. In these cases, the initial effective stress around the cavern is zero as it would be before the cavern was leached. The effective stress increases as the inside pressure is reduced. At the time the interior reaches brinehead pressure, the effective stress around the cavern is at a maximum, then it gradually dissipates with time to steady state effective stress. In all three cases, the steady state effective

stress distribution on the mesh is essentially the same and it corresponds to the steady state flow rate after 3000 days as shown in Figure 5. In all three cases, the flow rate at time zero results from the initial elastic response of the cavern. The 1000 day leaching period was used in all the subsequent cavern analyses presented in this report.

2.6 Simulating Cavern Leaching During Oil Withdrawal

The SPR is designed to allow five oil withdrawals of each cavern during the thirty year life of the program. When the oil is withdrawn, it is replaced by fresh water which leaches the cavern to a larger size. A computer program [11] for predicting leaching was obtained by the Fluid and Thermal Sciences Department at Sandia and modified to more closely meet SPR needs. This program [10] was used to predict the new cavern size after each oil withdrawal/leaching cycle. The cavern leaching was taken into account during the finite element analysis by predefining the model to match the layers which were predicted to be leached as shown in Figure 6. The timing of the five withdrawals is not known a priori since it will depend on the national energy situation at that time. For analytical purposes, the withdrawals were divided evenly over the life of the SPR program (30 years), which results in one withdrawal every six years. At the time the withdrawal occurs, the pressure is transferred from the current cavern surface to the newly created surfaces as the layer of leached elements is deleted. The cavern closure rate increases because the volume has increased. Figure 7 shows the total volume of Bryan Mound Cavern One plotted against time. Each step in the curve represents a volume increase due to leaching. After each volume Increase, the cavern continues to creep inward as shown in the close-up of one leaching cycle in Figure 8.

2.7 Temperature Effects

As can be seen in Equation (2) below, the creep rate is an exponential function of temperature. The fluid going into the cavern is assumed to be approximately 70°F and gradually heats to the in-situ temperature of the cavern (between 100°F and 130°F depending on depth). This has two effects. First, the fluid expands as it heats and flows from the cavern if the

wellhead is open, or the internal pressure increases if the wellhead is shut. Second, the fluid cools the walls of the cavern resulting in thermal contraction and temporary reduction in creep rate. The computer code has the capability to treat the thermal stress problem and also the thermal influence on creep. A thermal analysis of one cavern was performed with a separate computer code which simulated the initial placement of cool fluid in a cavern and subsequent injections of cool fluid for the drawdown/leaching cycles. This time dependent thermal field was included in the structural creep analysis of the cavern.

For comparison, the same analysis was also made without the time dependent thermal field but using a constant temperature corresponding to the average temperature of the salt. Immediately after the first cool fluid injection, the analysis which included the thermal field predicted a cavern closure rate which was 50% less than in the constant temperature analysis. Within three or four years, however, the predicted cavern closure rates were about the same. Including a thermal gradient in each cavern's structural analysis was difficult because the thermal boundary conditions were hard to define with existing data. Each subsequent analysis was performed with a constant, average temperature. It was felt that this gives a good representation of cavern performance three or four years after the time of injection.

2.8 Material Properties

The program uses an elastic constitutive model and a secondary creep strain model of the form.

$$\dot{\bar{e}} = A \exp(-Q/RT)\bar{\sigma}^{(n)} \qquad (2)$$

where

$\bar{e}$ = secondary effective creep strain rate
A = laboratory determined constant
Q = activation energy
R = universal gas constant
T = temperature in degrees Kelvin
a = effective stress
n = stress exponent

The coefficients in the above equation were determined by triaxial creep testing of salt and are given in Table I. The elastic properties were determined from standard triaxial compression tests and are also given in Table I.

Table I

Material Properties

Site	A (1/[(days)(psf)^n])	Q (Kcal/mole K)	n	E (psf)	
Bryan Mound					
salt	9.51E-17	12.1	3.62	6.80E8	.33
shale	--	--	--	1.48E7*	.29
caprock	--	--	--	1.48E7*	.29
overburden	--	--	--	2.00E4*	.33
West Hackberry					
salt	2.92E-23	12.0	4.90	4.60E8	.26
shale	--	--	--	1.48E7*	.29
caprock	--	--	--	1.48E7*	.29
overburden		--	--	2.00E4*	.33

* Reduced intact modulus as explained in Section 2.11.

where

E = Youngs' Modulus
u = Poissons' Ratio

2.9 Predicting Salt Fracture

A function which conservatively predicts the occurrence of rock salt fracture has been developed [9]. This function relates confining pressure and effective creep strain and becomes positive when the potential for fracture or crushing exists.

$$\phi = 150.0\ (\varepsilon - 0.023 - f(P)) \qquad (3)$$

$$f(P) = \begin{cases} 0.132 & \text{for } P > 1.256 \times 10^{5} \text{ psf} \\ (2.117 \times 10^{-6})P - (8.450 \times 10^{-12})P & \text{otherwise} \end{cases} \quad (4)$$

where

ϕ = fracture function

ε = creep strain

$P = (\sigma_1 + \sigma_2 + \sigma_3)/3.0$ (confining pressure)

f(P) = function of confining pressure

Potential problem regions around a cavern were assessed by post-processing the finite element results to determine if the function was positive anywhere in the mesh. The code currently has no means of redistributing stresses if fracture occurs during computations.

2.10 Volumetric Calculations

The wellhead provides the only access to a cavern and consequently it is the only location that can be used to monitor cavern response. Typical information obtained from an instrumented wellhead includes pressure increase when the wellhead is sealed, and flow volume when the wellhead is opened to reduce the pressure. The pressure increase comes from two sources: 1) Creep closure, which reduces the cavern volume, and 2) Fluid thermal expansion, produced when the oil is heated from injection temperature to cavern temperature at depth. The daily pressure increase and the bleed down volume are used to calculate a dally cavern volume change which we call cavern closure rate. The computed pressure increase due to creep closure is also a function of the compressibility of the brine and oil. The compressibility assumed for brine was 2.2×10^{-6} 1/psi and the compressibility assumed for oil was 5.55×10^{-6} 1/psi.

The finite element code computes the nodal displacements at the end of each time step specified by the user. The volume of the cavern at each time step is computed by a post-processing program which uses the coordinates and displacements at each node on the cavern surface. The volume and time data

can then be manipulated into cavern closure rates and pressure increases. The cavern closure rates and pressure increases predicted with this procedure do not include the contribution from thermal expansion of cavern fluid. Hence, the values given here tend to underpredict the measured data. Research is currently being conducted to quantify the pressure increase from fluid thermal expansion.

2.11 Analysis of Newly Leached Expansion Caverns

Leaching of new expansion caverns at West Hackberry and Bryan Mound has commenced. The new caverns have the same geometry and depth at each site but material properties vary from site to site. In these analyses the finite element mode 1 and boundary conditions were kept the same and the material properties were varied.

A standard expansion cavern is a tapered cylinder with the top diameter being slightly larger than the bottom. The caverns are designed to have an initial volume of approximately 11.0 MMbbl with 10 MMbbl for oil storage and 1 MMbbl as a brine buffer from which bleed down can occur. After five drawdown cycles the standard caverns will have a volume of approximately 20 MMbbl The roof will be conical with the angle from horizontal being approximately 30 degrees. The top of the cavern will be at a depth of about 2000 feet and the bottom of the cavern will be at 4000 feet. The finite element model of a standard expansion cavern is shown in Figure 9.

Recent studies have shown that leaching the large volume of the new caverns will significantly influence the vertical stress in the region above the caverns [9] This was determined using the finite element model of the entire West Hackberry dome shown in Figure 10. In this model, the caverns are approximately represented (since this is a two-dimensional axisymmetric model) with a central cylinder and two adjacent toroids. The influence of leaching on the stress state above the caverns is shown in Figure 11 where the initial lithostatic stress is compared with the vertical stress predicted at the end of the SPR life. Figure 12 shows the variation in the vertical stress with time 500 feet above the cavern as leaching takes place.

This vertical stress history was applied as a boundary condition to the top of the detailed finite element model shown in Figure 9.

The boundary conditions on the walls of the cavern approximated the stress history of the cavern by simulating leaching (section 2.5) over the first three years, leaving the cavern at brine head pressure for five years and then simulating a drawdown/leaching cycle every six years by deleting a layer of elements. The results for a standerd cavern at Bryan Mound and West Hackberry are given in Sections 3.7 and 4.7 respectively.

3. BRYAN MOUND SALT DOME ANALYSIS RESULTS

3.1 General Site Description

The Bryan Mound salt dome is located in Southeastern Texas near the city of Freeport. approximately two miles inland from the Gulf. The edges of the dome have been explored for oil since 1901, but the amount produced has been small The major use of the site has been production of sulphur from the caprock and brine from five leached caverns. These five caverns were acquired by the U.S. Department of Energy (DOE) in April, 1977 for use in the SPR program All of the caverns underwent certification studies between 1977 and 1979 and all were deemed suitable for oil storage except Cavern Three which appeared to have some fresh water circulation. New wells were drilled into the caverns to meet design injection and withdrawal requirements. and oil injection started in October, 1977 [2]. The five caverns at Bryan Mound were analyzed in the present study to confirm the structural safety of the caverns and to predict the volume losses from the caverns due to creep closure. Figure 13 shows 6 plan view of the Bryan Mound salt dome and the five existing caverns in relation to each other and to the edge of the dome.

3.2 Bryan Mound Cavern One

The well for Bryan Mound Cavern One was initially drilled in 1942. The volume of the cavern is currently 5 3 million barrels (MMbbl) (2.98 x 107 ft^3) The cavern is located well away from the edge of the dome and the

caprock, but has a pillar only 245 feet between it and Cavern Four. Caverns Four and Five are the only existing caverns that are on the same level as Cavern One. Two new caverns will be leached about 800 feet away and two more new caverns will be leached about 1000 feet from Cavern One and on the same level The shape and dimensions of the cavern 6s determined from sonar data are shown in Figure 14 [2]. The finite element model of Cavern One is shown in Figure 4 and has a volume of 5.0 MMbbl (2.80 x 10^7 ft^3). The volumetric response of the cavern versus time is given in Figure 7 and a summary of the predicted cavern closure rate immediately before each oil withdrawal is given in Table II

Calculation of the fracture function shows the cavern to be structurally sound and will continue 6s such through the first several drawdown cycles. There is 6 possibility of coalescence with cavern four on the second or third drawdown, requiring that the growth of both caverns be monitored closely [2]. Because of our two-dimensional approach, the present analysis will not predict the stresses or fracturing of the pillar as the two caverns approach each other.

TABLE II

Bryan Mound Cavern One Predicted Cavern Closure Rates

Withdrawal Number	Initial	1	2	3	4	5
Volume (x 10^7 ft^3)	2 80	3.29	3.90	4.56	5.27	6.00
Cavern Closure Rate (ft^3/day)	22.0	31.3	39.6	51.8	64.0	75.3

3.3 Bryan Mound Cavern Two

The initial well for Cavern Two was drilled in 1942 and the 5.5 MMbbl (3.09 x 10^7 ft^3) cavern shown in Figure 15 was subsequently developed.

Cavern Three is the only cavern (including the new caverns) on the same level as Cavern Two and it is located 450 feet away. The cavern is well away from the edge of the dome, but it is only 365 feet below the caprock. This distance has been found suitable by past and present finite element analyses [2]. The finite element model, as shown in Figure 16 has a volume of 4.9 MMbbl (2.75 x 107 ft^3). The volumetric response of the cavern versus time is given in Figure 17 and the predicted cavern closure rates immediately before each oil withdrawal are given in Table III.

Results from the fracture function show this cavern to be structurally sound throughout its entire SPR life including the five drawdown cycles.

TABLE III

Bryan Mound Cavern Two Predicted Cavern Closure Rates

Withdrawal Number	Initial	1	2	3	4	5
Volume (x 107 ft^3)	2.75	3.39	4.14	4.99	5.89	6.87
Cavern Closure Rate (ft^3/day)	6.4	7.8	12.7	20.0	35.8	29.0

3.4 Bryan Mound Cavern Three

Cavern Three was initiated in 1941 and currently has a volume of 6.4 MMbbl (3.59 x 107 ft^3). This cavern was purchased for oil storage along with the rest of the caverns, but was subsequently deemed unsuitable for this purpose Early in its testing, it appeared to have fresh water circulation and continual leaching taking place within the cavern. There are also problems with the well leaking and until both of these problems are fixed or reconciled, oil will not be stored in this cavern [2].

A finite element analysis of the cavern was carried out in the present study to confirm its structural stability over the life of the SPR program and to predict the creep closure rate of the cavern.

The Cavern, shown in Figure 18, is relatively shallow and Cavern Two is the only other cavern on the same level. The finite element mesh, which has a cavern volume of 12.76 MMbbl (7.16×10^7 ft^3), is shown in Figure 19. The mesh was made using the largest cross-section found in the sonar surveys, because showing that this larger cavern is structurally sound would also indicate the safety of the actual cavern. The fracture function shows this cavern to be stable throughout the life of the SPR program. The analysis predicts a loss of approximately two percent of the original volume over sixty years. Unfortunately, there does not seem to be any closure rate data for comparison

3.5 Bryan Mound Cavern Four

Cavern Four is the second largest cavern in the SPR program with a volume of 16.3 MMbbl (9.15×10^7 ft^3). The well for this cavern was drilled in 1942 and gradually developed into the shape shown in Figure 20. This cavern is approximately in the center of the dome and is 1500 feet below the caprock so no edge of dome or roof thickness problems are anticipated. Caverns One and Five are on the same level and relatively close (pillar thicknesses of 245 feet and 320 feet, respectively). Three of the new expansion caverns are also on the same level and within approximately 1100 feet [2]. The finite element mesh shown in Figure 21 has a cavern volume of 16.9 MMbbl (9.49×10^7 ft^3). The predicted cavern closure rate immediately before each drawdown is given in Table IV and the total volume versus time is plotted in Figure 22.

Post-processing of the fracture function indicates the present and future (after five drawdown cycles) stability of this cavern. There is the possibility of coalescence with Cavern One, as mentioned previously and also with Cavern Five [2]. The volume growth and pillar distances between these three caverns needs to be closely monitored.

TABLE IV

Bryan Mound Cavern Four Predicted Cavern Closure Rates

Withdrawal Number	Initial	2	3	4	5
Volume (x 10^7 ft^3)	9.49	10.63	12.17	13.86	15.68	17.44
Cavern Closure Rate (ft^3/day)	160.1	206.7	271.5	340.0	423.1	503.8

3.6 Bryan Mound Cavern Five

Cavern Five was initiated in 1957 and subsequently developed into the 33.4 MMbbl (1.88 x 10^8 ft^3) cavern shown in Figure 23 The cavern has an upper and lower lobe separated by what appears to be an insoluble layer (the 1 edge may be the result of non-uniform leaching with depth rather than insolubi 1 i ty) This cavern is the largest in the SPR program, but since it 1s over 650 feet from the dome edge and 1000 feet from the caprock, no dome edge or roof thickness problems are anticipated. Cavern Four and two new expans ion caverns are located o n the same level as this cavern. Also included as a factor in the determination of the mesh width was the distance to the edge of the dome [2]. The finite element representation of the cavern in Figure 24 has a volume of 33.4 MMbbl (1.88 x 10^8 ft^3). This mesh does not include a layer of elements for deletion with each drawdown. An at tempt was made to include the layers. but the resulting mesh was so fine and had so many elements as to make the analysis overly computer time intensive. The present mesh has one layer of elements between the original and final size The volumetric response of the cavern is given in Figure 25 and a summary of the predicted cavern closure rate after the first and final drawdown is given in Table V

The post-processed fracture function does not indicate any stability probiems of the cavern at present or in the future As mentioned

previously. there is the possibility of coalescence with Cavern Four. The present model is not suitable for predicting pillar stability problems associated with this coalescence process

TABLE V

Bryan Mound Cavern Five Predicted Cavern Closure Rates

Withdrawal Number	Initial	1	2	3	4	5
Volume (x 10^7 ft^3)	18.8			----		26.3
Cavern Closure Rate (ft^3/day)	448.8					849.6

3.7 Bryan Mound Expansion Caverns

In addition to the existing caverns, current efforts are underway to leach standard expansion caverns at the Bryan Mound site. A description of the methods used to analyse this standard cavern is given in section 2.11. The predicted closure rate of a standard cavern where Bryan Mound material properties were used is given in Table VI and the total volume versus time is shown in Figure 26.

Post-processing of the computational results using the fracture function show that the standard cavern at Bryan Mound is stable' throughout its SPR life including the five drawdown cycles.

TABLE VI

Bryan Mound Expansion Cavern Predicted Cavern Closure Rates

Withdrawal Number	Initial	1	2	3	4	5
Volume (x 107 ft^3)	6.15	7.18	8.11	9.43	10.79	12.13
Cavern Closure Rate (ft^3/day)	162.5	296.0	317.3	431.0	673.4	720.2

4. WEST HACKBERRY SALT DOME ANALYSIS RESULTS

4.1 General Site Description

The West Hackberry SPR Site is located about 75 miles southwest of Lake Charles, LA. Calcasieu Lake, which has a surface area of approximately 75 square miles, is directly east of the site about five miles. Black Lake, which is immediately north of the site, originally had an area of about four square miles but has increased its' area in the past 30 years to between 25 and 50 square miles. Subsidence at the site is probably the cause of the increase.

The site was first explored for oil in 1902 and has had a long and fruitful history. The first oil discovery was in 1928 when a trap was found on the flank of the dome. During this time sulphur exploration was begun but there is no evidence that sulphur mining was ever pursued.

In 1934 Olin Corporation began producing chemical feedstock brine from wells drilled into the salt. Five of these caverns were obtained by DOE and used as initial storage for the SPR program. The dome is a large one with several other commercial interests at the site. There are eleven hydrocarbon storage caverns owned by Cities Services on 80 acres southeast of the present SPR site [12]. A cross-section of the West Hackberry Salt Dome is shown in Figure 27.

4.2 West Hackberry Cavern Six

The well for Cavern Six was drilled in 1946 and it was developed as a brine feedstock cavern. The cavern was obtained by DOE for the SPR and was first certified in 1977. It is has a regular pan shape with a volume of 7.1 MMbbl, a height of 153 feet and a maximum diameter of 1150 feet. The maximum diameter IS at the top of the cavern in a thin pancake-like cavity. This cavity is about ten feet high and 1150 feet in diameter. The majority of the cavern has a diameter of about 800 feet.

Cavern Six is approximately 1200 feet below the caprock and about 700 feet from the edge of the dome. Caverns Seven, Eight and Nine and two standard expansion caverns are on the same level and close enough to be included in the mesh width determination. The geometrical shape of the cavern is shown in Figure 28 [12] and a blow-up of the finite element mesh is shown in Figure 29. This cavern was analysed initially with leaching allowed in the thin pancake-like cavity. Leaching in this region expands the roof diameter even further and may threaten the stability of the cavern. Maintaining an oil blanket on the roof and down below the opening to the cavity when drawdowns occur will prevent further leaching of the cavity. The final cavern analysis was made assuming that leaching does not take place in the cavity at the top of the cavern.

The predicted cavern closure rates are given in Table VII and the total volume versus time is plotted in Figure 30. The computed pressure increase for this cavern is 3.12 psi/day whereas the measured pressure increase is approximately 1.14 psi/day. The discrepancy most likely results from a modeling problem such as. 1) the assumed temperature field around the cavern is too high giving an overprediction of creep rate, 2) the stress above the cavern has been significantly relieved through creep or 3) the mesh needs to be wider. The same temperature gradient and stress state were assumed in the analyses of Caverns Seven, Eight and Nine which are relatively close to Cavern Six and these all compared favorably with field data in terms of pressure increase per day. Unlike most caverns, the cavern closure rate for this cavern drops slightly after the second drawdown and increases with subsequent drawdown cycles. This is due to the fact that the

material leached is along the slanting side of the cavern which is not creeping as fast as the roof and floor. In the meantime the creep closure rate continues to decrease with time and this decrease with time more than offsets the increased closure rate due to deleting elements. The post-processing of the fracture function and minimum stresses show this cavern to be stable as long as leaching is prevented in the cavity around the roof.

TABLE VI I

West Hackberry Cavern Six Predicted Cavern Closure Rates

Withdrawal Number	Initial	1	2	3	4	5
Volume (x 10^7 ft^3)	3.89	4.62	5.30	6.00	6.74	7.51
Cavern Closure Rate (ft^3/day)	664.0	636.0	655.4	703.5	722.1	724.7

4.3 West Hackberry Cavern Seven

The well for Cavern Seven was drilled in 1946. Its geometry is a cyl inder sitting on a circular bulb. The cylinder is about 250 feet in diameter and 600 feet high. The circular bulb is about 430 feet in diameter. The cavern has a storage volume of 12.3 MMbbl making it the largest cavern at West Hackberry. It is about 500 feet below the caprock and at least 1000 feet from the edge of the dome. The closest cavern is No. six from which it IS separated by 545 feet. Cavern Eight is also located on the same level 750 feet away. The distances to Cavern SIX, Cavern Eight and the edge of the dome were used to determine the mesh width [12]. The geometry of the cavern is shown in Figure 31 and the finite element mesh is shown in Figure 32.

Predictions of the volume loss of the cavern due to creep closure is given in Table VIII and total volume versus time is plotted in Figure 33. Calculations of the fracture function show this cavern to be structurally sound throughout its entire SPR life including the five drawdown cycles.

The separation distances from the edge of the dome and Cavern Six indicate that there should be no interaction of this cavern with No. Six or the edge of the salt throughout the five drawdown cycles.

TABLE VIII

West Hackberry Cavern Seven Predicted Cavern Closure Rates

Withdrawal Number	Initial	1	2	3	4	5
Volume (x 107 ft^3)	5.75	7.01	8.39	9.81	11.40	13.06
Cavern Closure Rate (ft^3/day)	98.0	164.6	242.4	374.1	554.8	833.4

4.4 West Hackberry Cavern Eight

The well for Cavern Eight was drilled in 1946. The geometry is a long slender cylinder on top of a shorter wider cylinder. The top cylinder has a diameter of 250 feet and a length of 800 feet. The bottom cylinder has a diameter of 446 feet and a height of 200 feet. The cavern has a volume of 10.1 MMbbl and is located 500 feet below the caprock and over 1000 feet from the edge of the dome. It is surrounded by caverns on the same level including, Six, Seven, Nine, Olin 3, Olin 5 and standard expansion caverns 101, 103 and 105. All of these caverns were used to determine the mesh width. Most of these caverns are over 1000 feet away but the separation distance to Nine is only 160 feet. These two caverns will likely coalesce during the third fresh-water refill cycle [12]. The geometry of this cavern is shown in Figure 34 and the finite element mesh in Figure 35.

Predictions of the volume change due to creep closure are given in Table IX and the total volume versus time is plotted in Figure 36. Calculation of the fracture function shows this cavern to be stable throughout its SPR life. The growth of this cavern and Cavern Nine should

be monitored closely after the second drawdown and further analysis of the stability of the separating pillar performed at that time.

TABLE IX

West Hackberry Cavern Eight Predicted Flow Rates

Withdrawal Number	Initial	1	2	3	4
Volume (x 10^7, ft^3)	5.42	6.27	7.12	8.15	9.10
Cavern Closure Rate (ft^3/day)	129.5	148.7	181.0	252.8	336.9

4.5 West Hackberry Cavern Nine

The well for Cavern Nine was drilled in 1947. It has a geometry consisting of two chambers. The upper chamber is approximately 400 feet in diameter at the top and necks down to about 60 feet in diameter. The lower chamber is a cylinder approximately 588 feet in diameter. The 1977 sonar survey taken on certification was 8.9 MMbbl. The cavern geometry is shown in Figure 37 and the finite element model is shown in Figure 38. After certification the cavern was brined again by Olin and has not been resurveyed. The cavern is located far from the edge of the dome and more than 1000 feet below the caprock. The pillar distance to Cavern Eight is approximately 160 feet and the two will probably coalesce before three fresh-water drawdowns. Caverns Six, Seven, 103, 109 and 110 surround Cavern Nine and their pillar distances were used in calculating the mesh width [12]

Predictions of the volume change due to creep closure are given in Table X and the total volume versus time is plotted in Figure 39. Calculation of the fracture function shows this cavern to be stable throughout its entire SPR life. As mentioned in the section on Cavern Eight, the growth of these two caverns should be monitored closely since coalescence is likely to occur after the third drawdown.

TABLE X

West Hackberry Cavern Nine Predicted Flow Rates

Withdrawal Number	Initial	1	2	3	4	5
Volume (x 10^7 ft^3)	4.45	5.32	6.25	7.25	8.30	9.22
Cavern Closure Rate (ft^3/day)	120.9	170.8	244.4	341.4	477.3	638.7

4.6 West Hackberry Cavern Eleven

The well for Cavern Eleven was drilled in 1962. It has a cylindrical geometry with a diameter of 306 feet, a height of 815 feet and a volume of 8.5 MMbbl based on the June 1977 sonar survey. It is well away from the edge of the dome and well below the caprock. It is also more than 1000 feet from the closest cavern [12] so the width of the finite element mesh was chosen to simulate an infinite boundary. The geometry of the cavern is shown in Figure 40 and the finite element mesh is shown in Figure 41.

The predicted cavern flowrates for the five drawdown cycles are given in Table XI and the total volume versus time is plotted in Figure 42. post-processing of the fracture function shows this cavern to be stable throughout its entire SPR life including the five drawdown cycles.

TABLE XI

West Hackberry Cavern Eleven Predicted Flow Rates

Withdrawal Number	Initial	1	2	3	4	5
Volume (x 107 ft^3)	4.38	5.04	5.73	6.48	7.27	8.11
Cavern Closure Rate (ft^3/day)	81.7	112.3	138.1	171.1	212.1	266.0

4.7 West Hackberry Expansion Caverns

In addition to the existing caverns, current efforts are underway to 1 each expans i on caverns at the West Hackberry site. A description of the methods used to analyse this standard cavern is given in Section 2.11. The predicted closure rate of a standard cavern using West Hackberry material properties is given in Table XII and the total volume versus time is shown in Figure 43.

Post-processing of the computational results using the fracture function show that the standard cavern at West Hackberry is stable throughout its SPR life including the five drawdown cycles.

TABLE XI I

West Hackberry Expansion Caverns Predicted Flow Rates

Withdrawal Number	Initial	1	2	3	4	5
Volume (x 10^7 ft^3)	6.15	7.18	8.11	9.43	10.79	12.13
Cavern Closure Rate (ft^3/day)	143.7	298.4	342.1	499.0	717.3	947.0

5. COMPARISON WITH FIELD DATA

Field data from caverns which currently hold oil has become available in the past few months. The data is not precise in that it comes from daily wellhead pressure readings on 1000 psi dial gauges. However, when many months of data are digitized and analyzed by a computer, some general trends can be obtained. The measured pressure increase shown in Table XIII is the result of averaging the slopes of several multimonth pressure versus time curves derived from field data. The finite element prediction of the pressure increase for each cavern and the ratio between the predicted and measured pressure increase are also given in Table XIII.

With the exception of West Hackberry Cavern 6, Table XIII shows that the computed pressure increase is always less than the measured pressure increase. The flll dates for each of the caverns indicate a relatively short time has elapsed since fill was completed and that the caverns are probably not yet approaching thermal equilibrium. This means that a (as yet unquantified) portion of the measured pressure increase is due to fluid thermal expansion. The mean and standard deviation in Table XIII show that the comparison is fairly consistent. The relatively large difference in the data from Bryan Mound Cavern One, West Hackberry Cavern Six and West Hackberry Cavern Seven could be due to: 1) spatially varying material properties, 2) the axisymmetric finite element mesh not modeling the real cavern very well, 3) thermal fluid expansion is larger for this cavern, or 4) the field data has some erroneous values. It is apparent that the contribution to the pressure increase from fluid thermal expansion needs further study and quantification.

TABLE XIII

Comparison of Finite Element Predictions and Field Data

Cavern	Fill Dates	Meas. Pres. Inc (psi/day)	Computed Press. Inc. (psi/day)	Comp./Meas.
BM1	10/78 - 10/82	0.55	0.15	0.27
BM2	10/77 - 10/79	0.093	0.048	0.52
BM4	11/77 - 8/81	0.66	0.33	0.50
BM5	5/78 - 6/81	0.78	0.48	0.62
WH6	8/77 - 11/81	1.14	3.12	2.74
wH7	10/78 - 7/80	1.45	0.32	0.22
WH8	10/78 - 4/80	0.65	0.43	0.66
WH9	7/78 - 6/79	1.20	0.50	0.38
WH11	7/77 - 11/80	1.10	0.34	0.31

Mean of Comp./Meas. = 0.435
Standard deviation of Comp./Meas. = 0.164
} (excluding WH6)

6. CONCLUSIONS

The methods presented in this report for determining creep response of leached salt caverns work reasonably well considering the limitations of two-dimensional approximations of the actual shapes and boundary conditions. The relatively consistent comparison of finite element predictions and limited field data also shows that the method is valid. The volume change versus time data, which have been predicted, will be useful to cavern operators in the planning of bleed down schedules, brine buffer sizes, and disposal of brine displaced from the cavern due to creep closure. This aid in predicting and planning should result in a more efficient cavern operation.

The analytical techniques employed show that the West Hackberry and Bryan Mound Caverns in the SPR are currently structurally sound and with few exceptions are expected to remain structurally sound through the planned drawdown cycles. Those few caverns which may develop problems are discussed in their respective sections and operating procedures to enhance long-term structural stability are described.

7. ACKNOWLEDGEMENTS

The thermal analyses used to study temperature effects were done by A. J. Russo, Sandia National Laboratories, Division 1512. C. M. Stone, Sandia National Laboratories, Division 1521, implemented the element removal capability into the computer code. The field data was obtained by POSSI, the cavern operating company and processed by R. R. Beasley, and C. A. Searls, Sandia National Laboratories, Division 6257.

8. REFERENCES

1 Hart, R. J., Ortiz, T. S., Magorian, T R., 1981, Strategic Petroleum Reserve (SPR) Geological Site Characterization Report Big Hill Salt Dome, Sandia National Laboratories, SAND81-1045, September, 1981.

2. Hogan, R. G., Strategic Petroleum Reserve Geological Site Characterization Report Bryan Mound Salt Dome, Sandia National Laboratories, SAND80-7111, October, 1980.

3. Hogan, R. G., Strategic Petroleum Reserve (SPR) Geological Site Characterization Report Bayou Choctaw Salt Dome, Sandia National Laboratories, SAND80-7140, December, 1980.

4. Key, S. W., Stone, C. M., and Krieg, R. D., A Solution Strategy for the Quasi-Static Large Deformation Inelastic Response of Axisymmetric Solids, presented at U.S. European Workshop Nonlinear Finite Element Analysis Structural Mechanics, Ruhr Universitat, Bochum, W. Germany, 1981.

5. Miller, J. D., Stone, C. M., and Branstetter, L. J., Reference Calculations for Underground Rooms of the WIPP, Sandia National Laboratories, SAND82-1176, August, 1982.

6. Morgan, H. S., Krieg, R. D., and Matalucci, R. V., Comparative Analysis of Nine Structural Codes Used in the Second WIPP Benchmark Problem, Sandia National Laboratories, SAND81-1389, November, 1981.

7. Preece, D. S., and Stone, C. M., Use of Laboratory Triaxial Creep Data and Finite Element Analysis to Predict Observed Creep Behavior of Leached Salt Caverns, Sandia National Laboratories, SAND82-0678, August, 1982.

8. Preece, D. S., and Stone, C. M., Verification of Finite Element Methods Used to Predict Creep Response of Leached Salt Caverns, Proceedings of 23rd Symposium on Rock Mechanics, Berkeley, CA, August, 1982.

9. Preece, D. S , and Wawersik, W. R., " Leached Salt Cavern Design Using a Fracture Criterion for Rock Salt," Proceedings of 25th Symposium on Rock Mechanics, Evanston, Illinois, June, 1984.

10. Russo, Anthony J., A Solution Mining Code for Studying Axisymmetric Salt Cavern Formation, Sandia National Laboratories, SAND81-1231, September, 1981.

11. Saberian, A., and Podio, A. L., A Computer Model for Describing the Development of Solution-Mined Cavities, IN SITU, l(l), p. l-36, 1977.

12. Wawersik, W. R., Hannum, D. W., Lauson, H.S., Compression and Extension data for Dome Salt from West Hackberry, Louisiana, Sandia National Laboratories, SAND79-0668, September, 1980.

13 Wawersik, W. R , Holcomb, D. J., Hannum, D W.. Quasi-Static and Creep Data for Dome Salt From Bryan Mound, Texas, Sandia National Laboratories, SAND80-1434, November, 1980.

14. Whiting, G. H., Strategic Petroleum Reserve (SPR) Geological Site Characterization Report West Hackberry Salt Dome, Sandia National Laboratories, SAND80-7131, December, 1980.

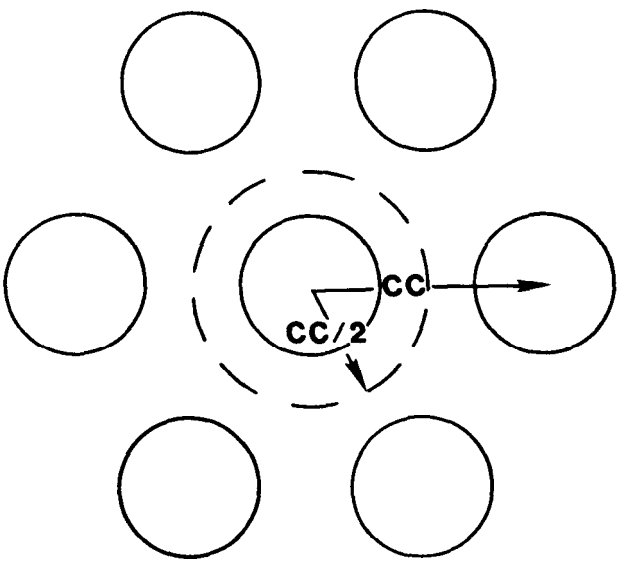

Figure 1: Top View of Cylindrical Cavern Array

3%

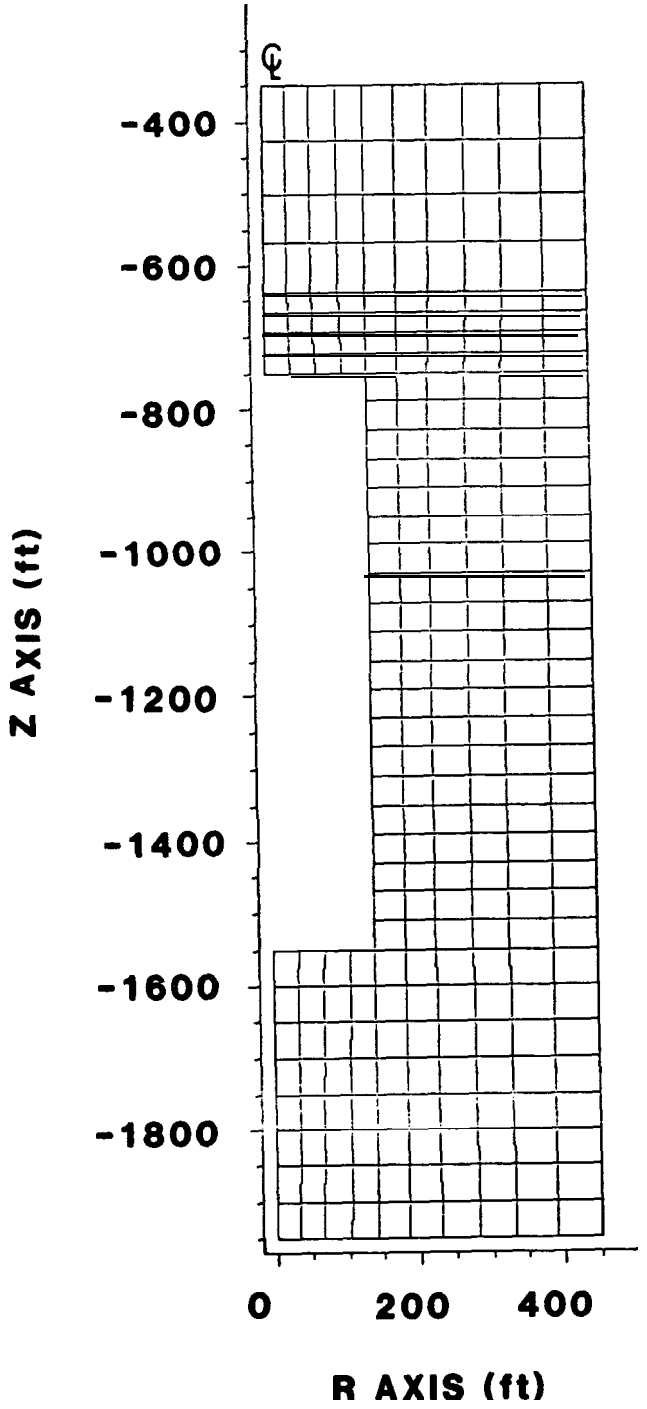

Figure 2: Axisymmetric Finite Element Model of Cylindrical Cavern.

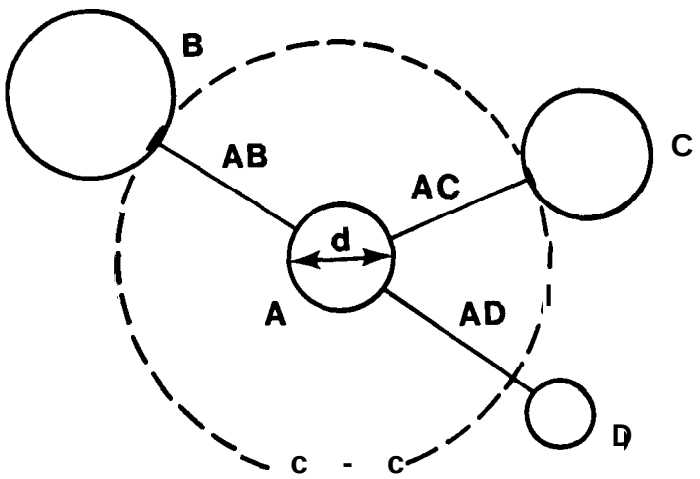

Figure 3 Top View of Typical Cavern Group

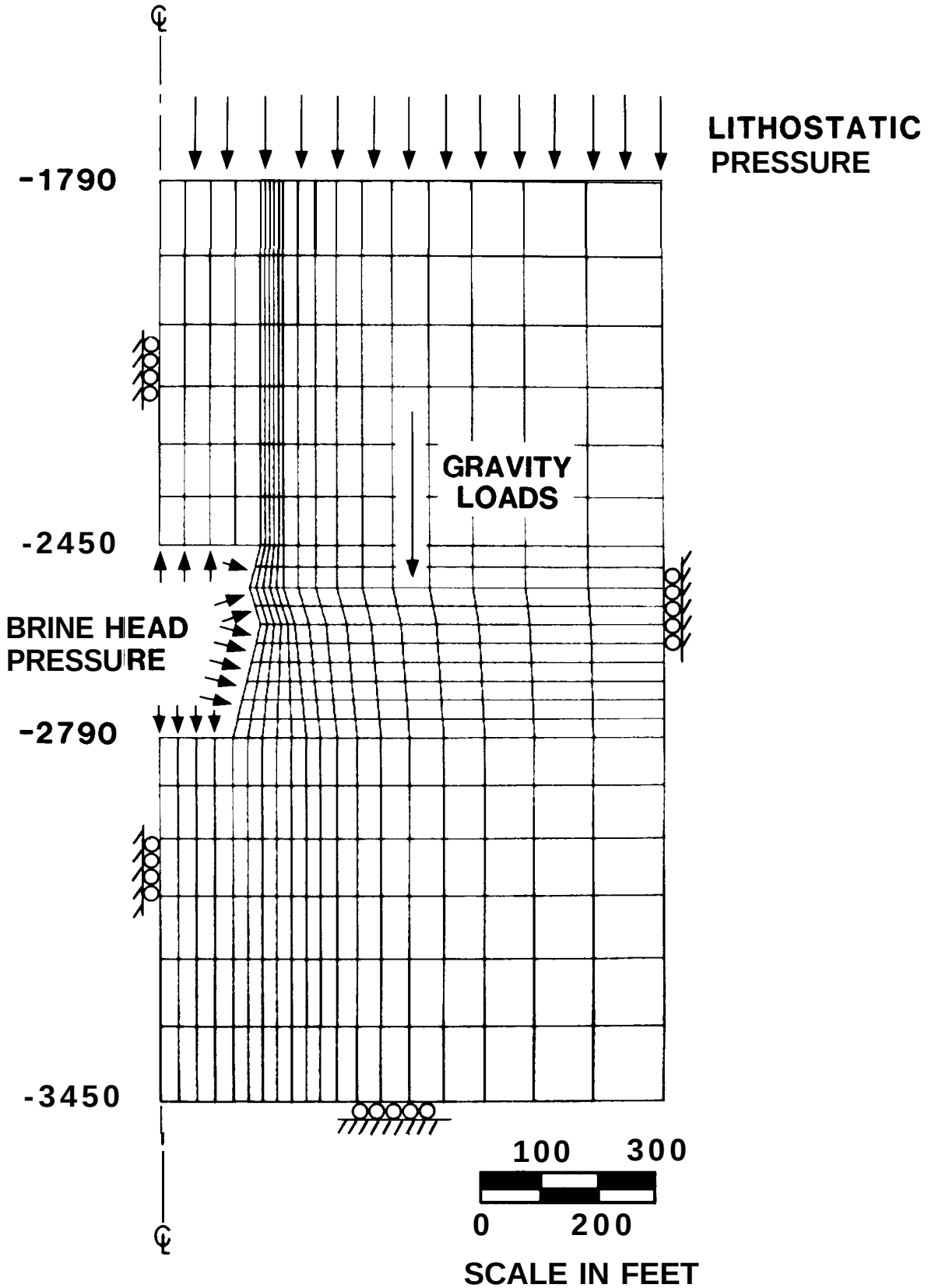

Figure 4. Axisymmetric Finite Element Model of Bryan Mound Cavern One.

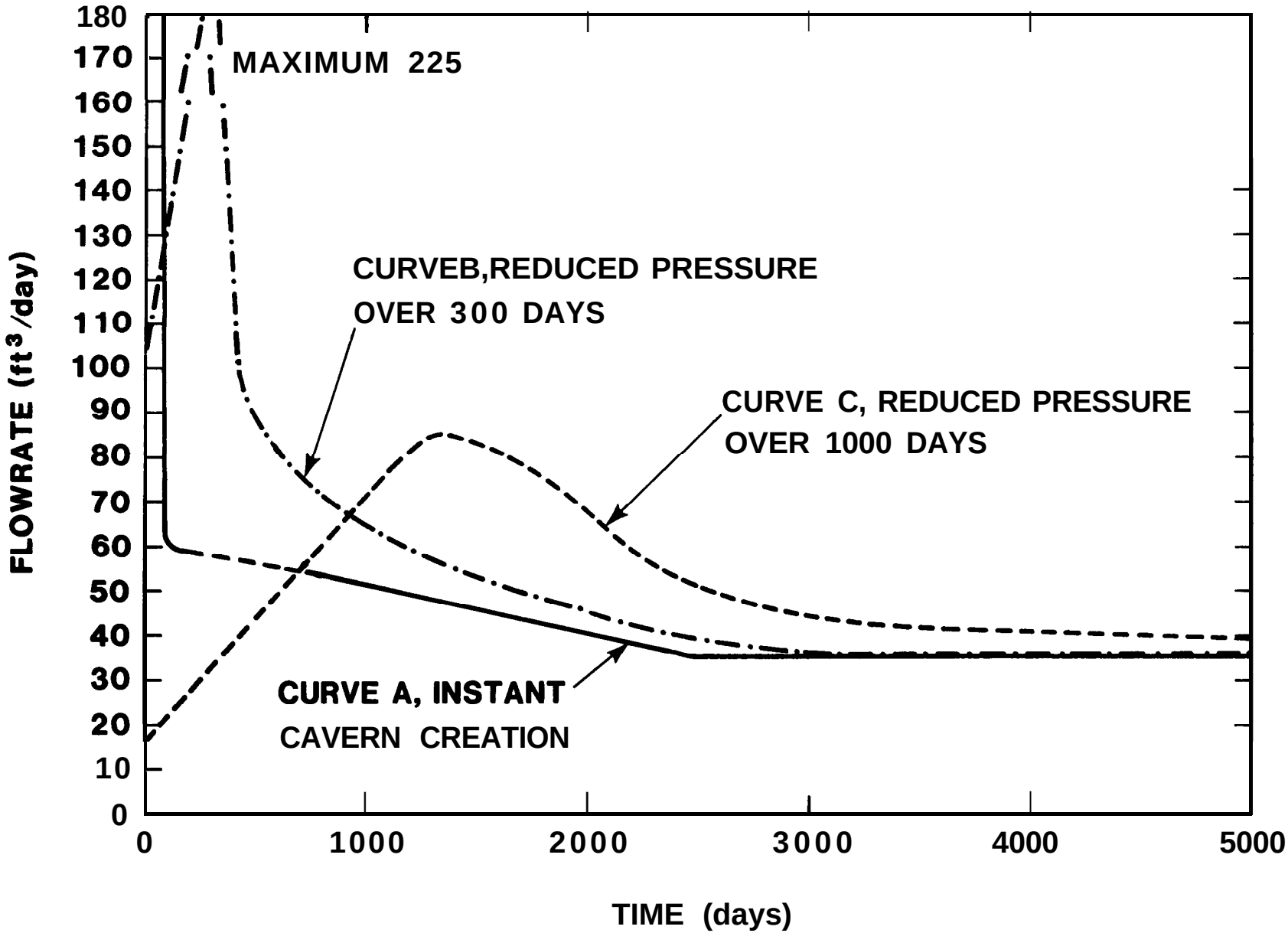

Figure 5. Flowrate Versus Time For Three Different Treatments of the Initial Leaching Process

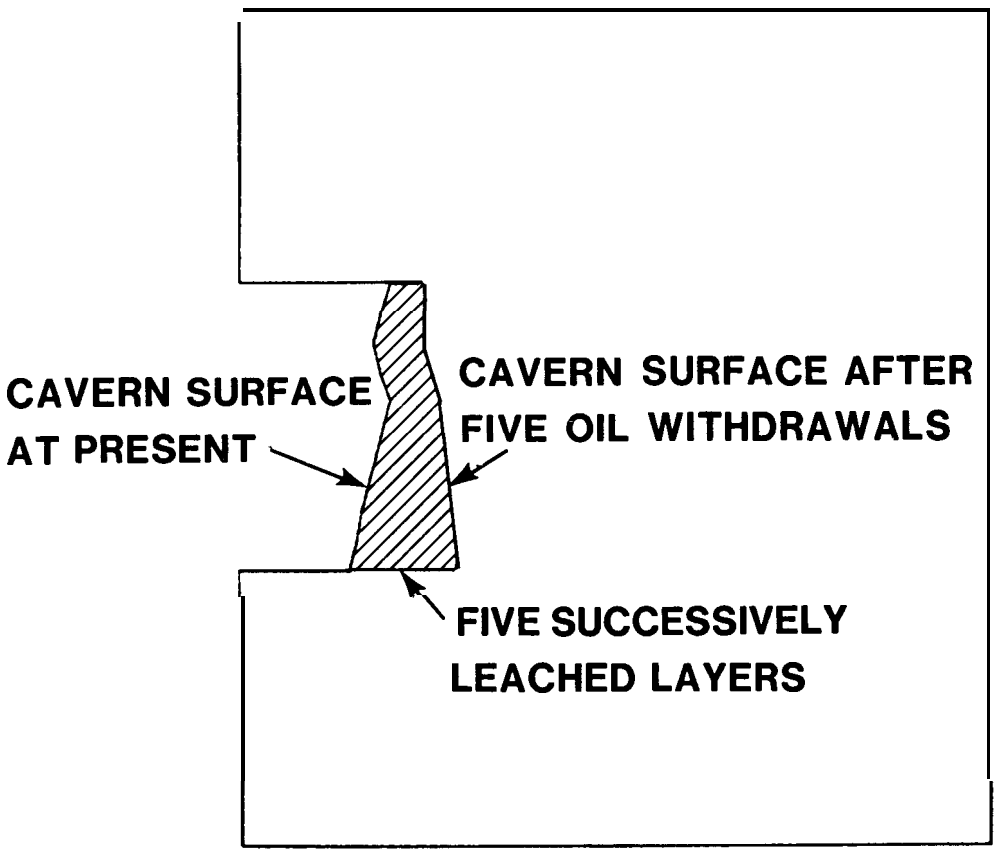

Figure 6 Bryan Mound Cavern One With Leached Layers Crosshatched.

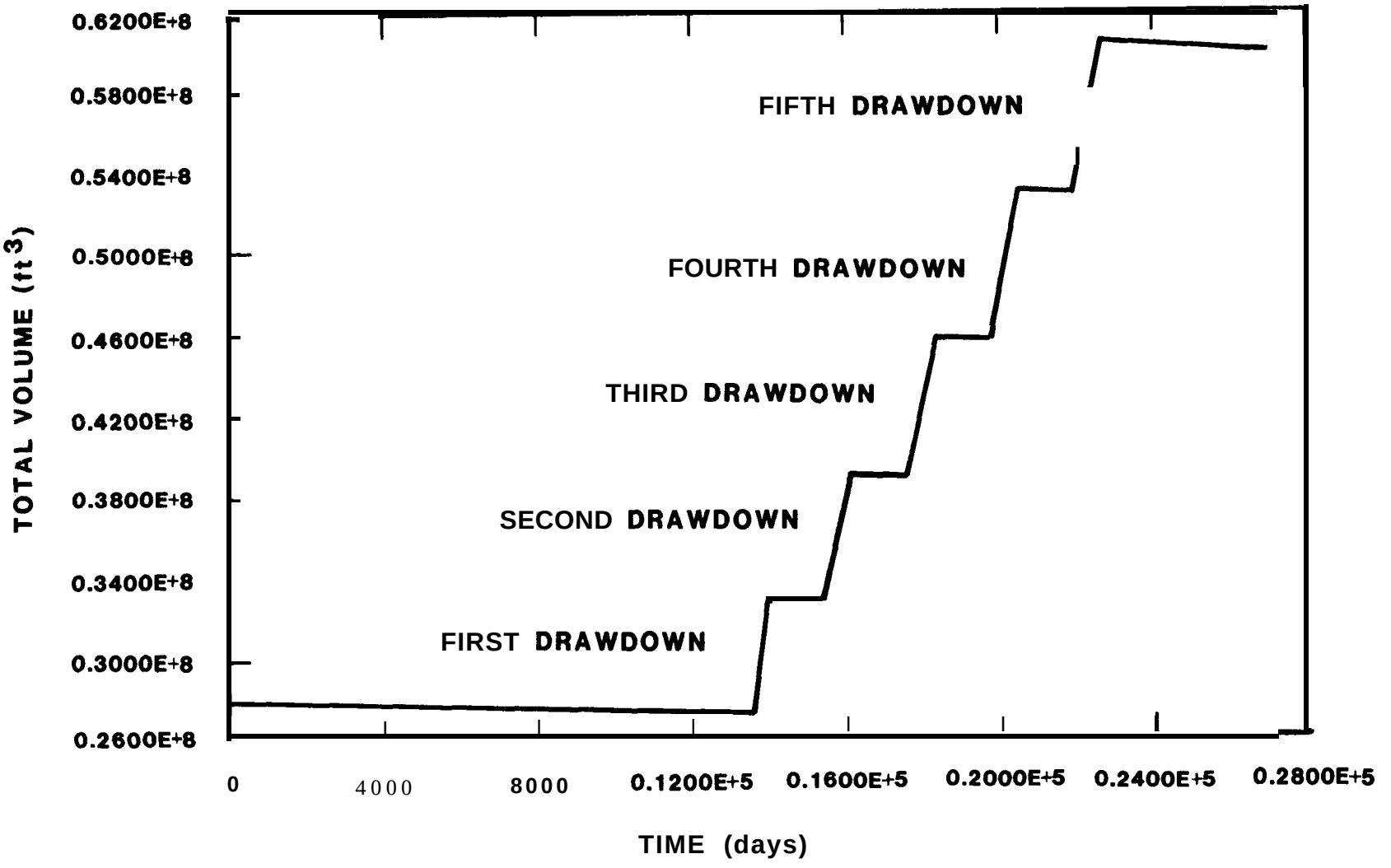

Figure 7 Volumetric Response of Bryan Mound Cavern One

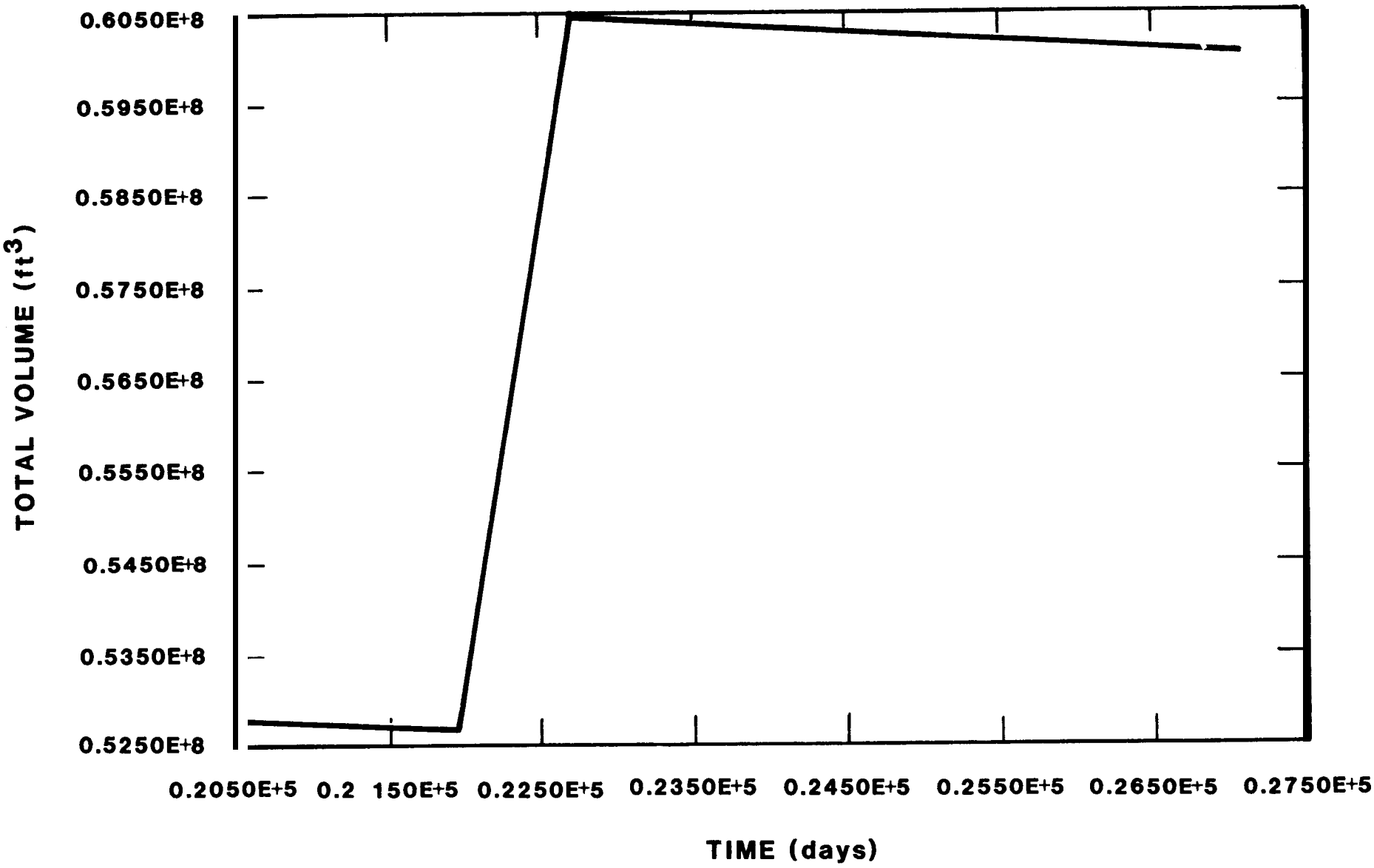

Figure 8 Final Leaching Cycle of Bryan Mound Cavern One

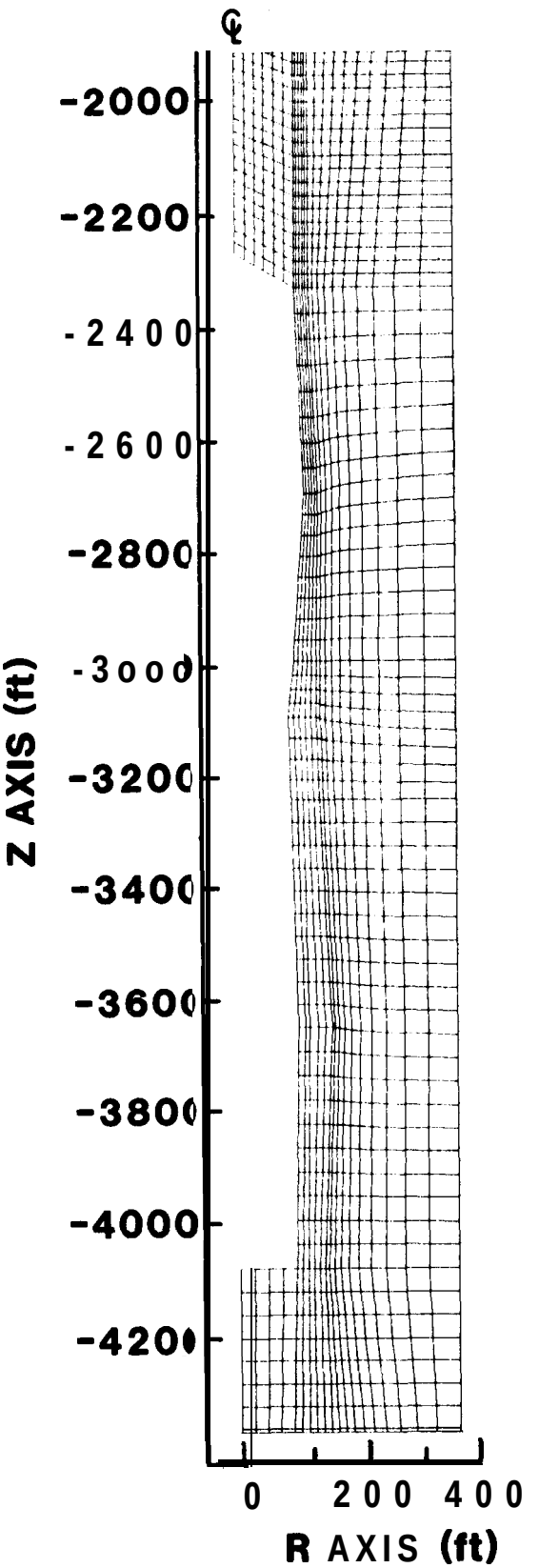

Figure 9. Close up of Axisymmetric Finite Element Model of Standard Expansion Cavern.

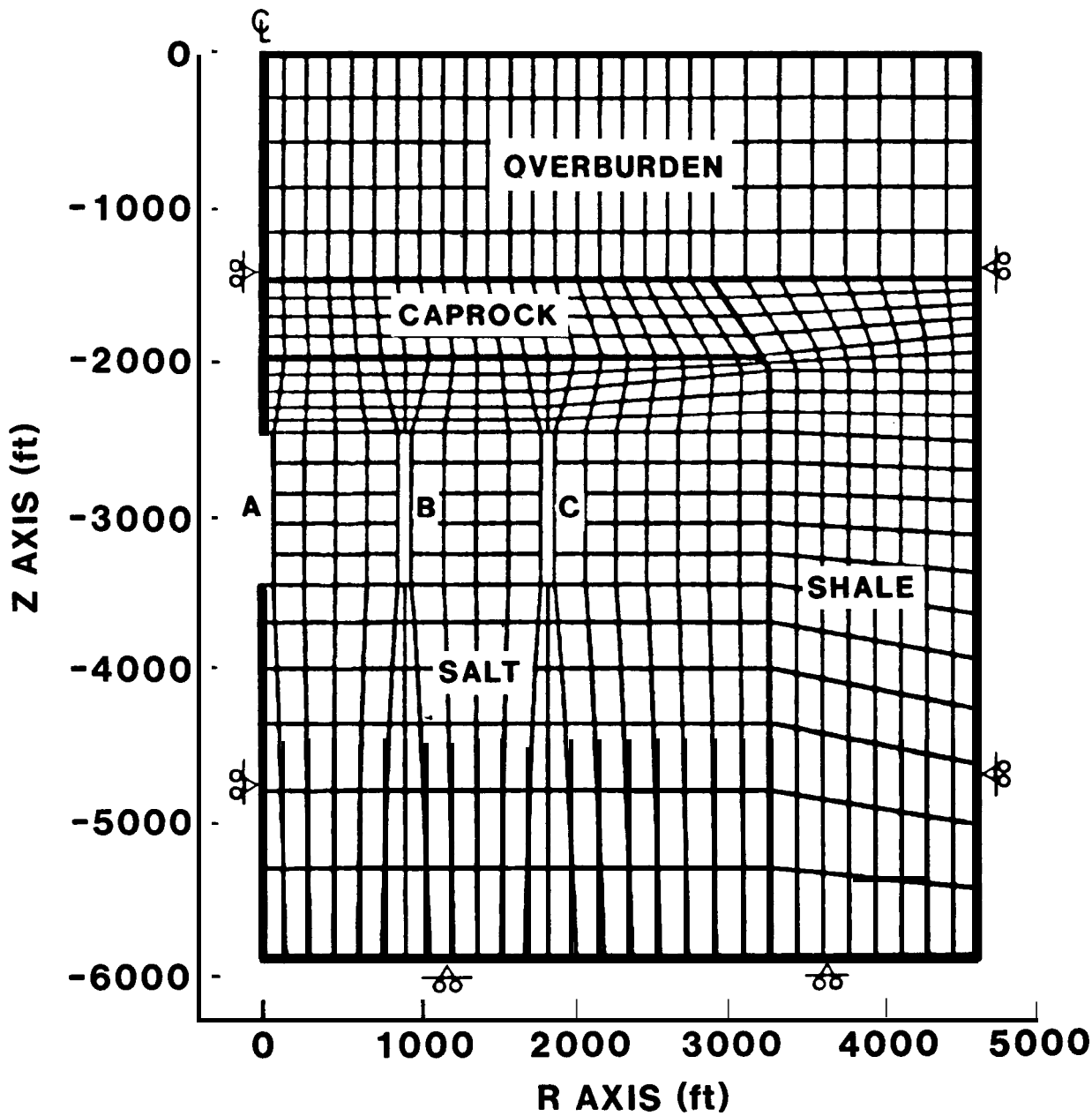

Figure 10: Axlsymmetric Finite Element Model of Wes Hackberry Salt Dome.

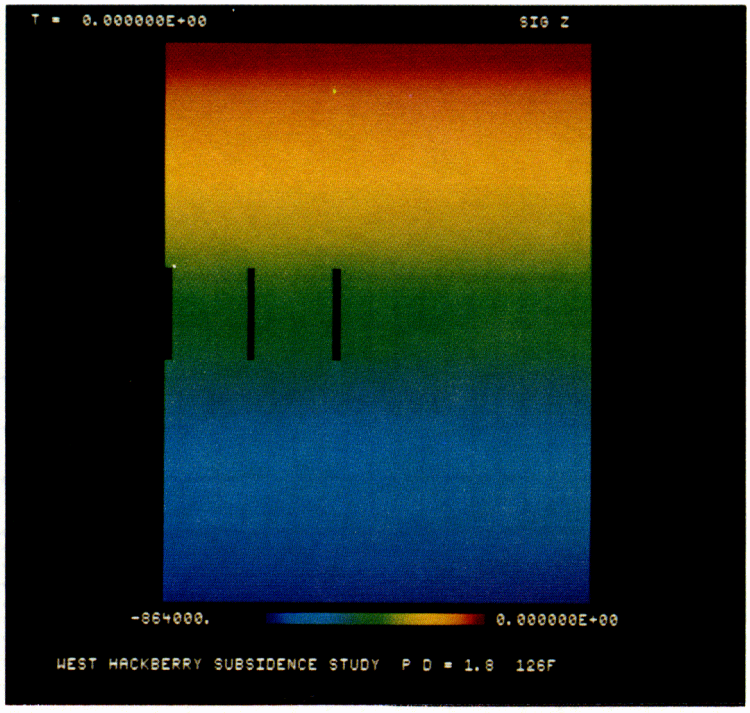

Figure 11a: Lithostatic Stress In West Hackberry Salt Dome

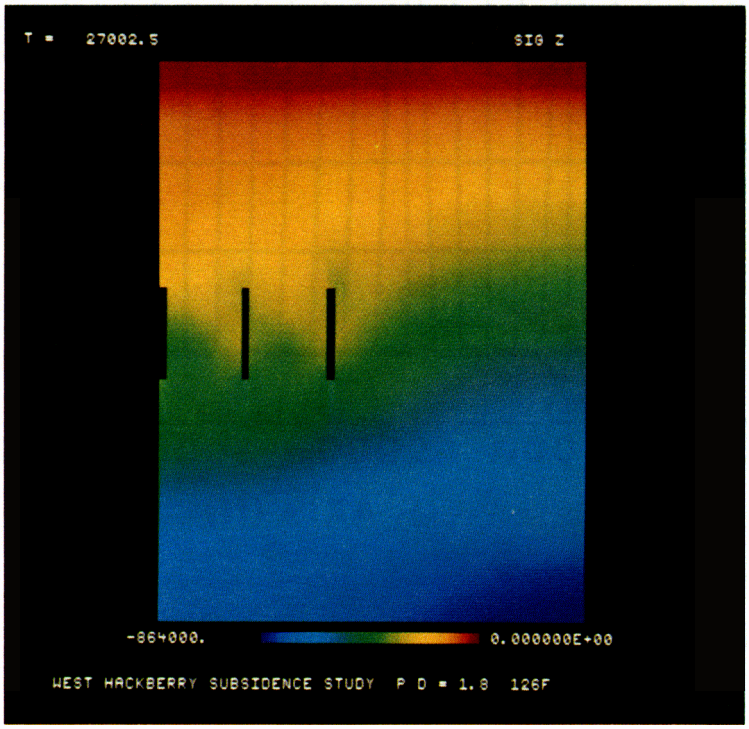

Figure 11b: Vertical Stress In West Hackberry Salt Dome At End Of SPR Life.

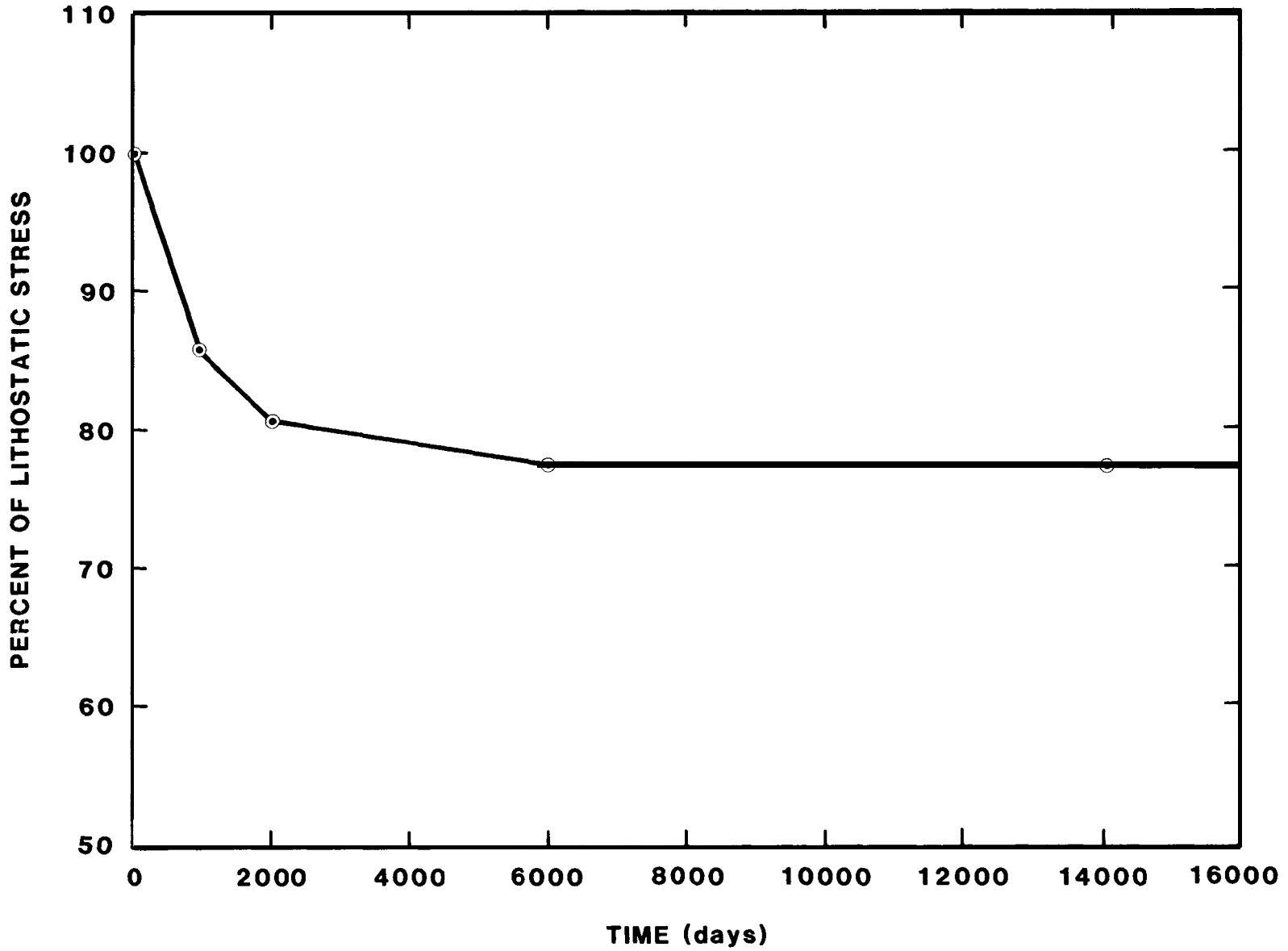

Figure 12: Vertical Stress Versus Time 500 Feet Above Toroid B.

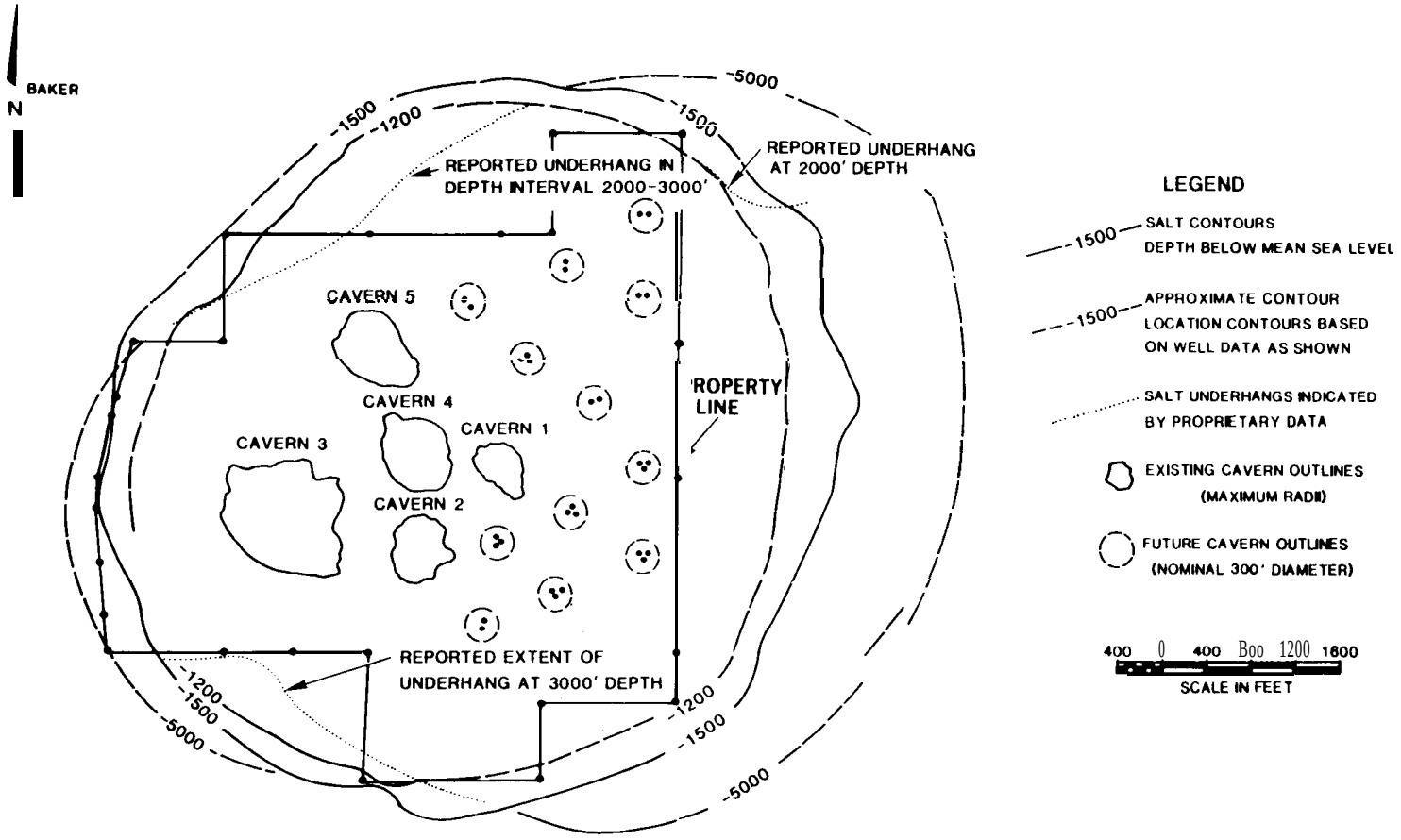

Figure 13 Plan View of Bryan Mound Salt Dome.

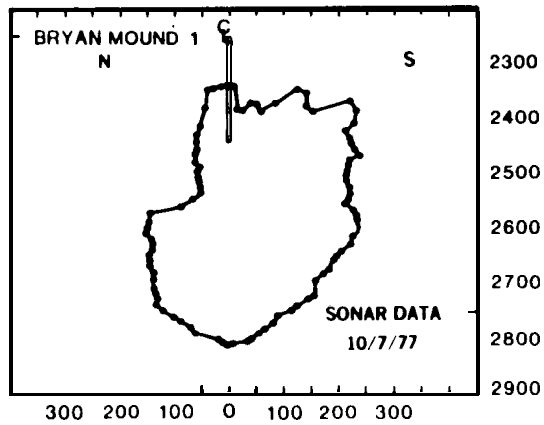

a SONAR PROFILE

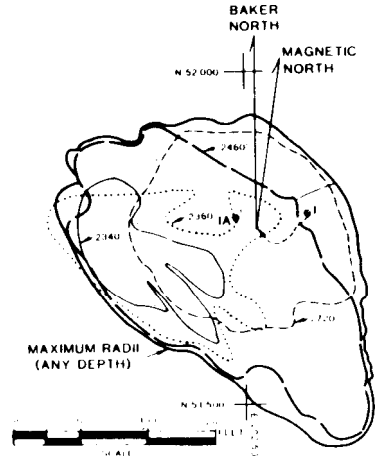

b HORIZONTAL SECTIONS (SEC. II)

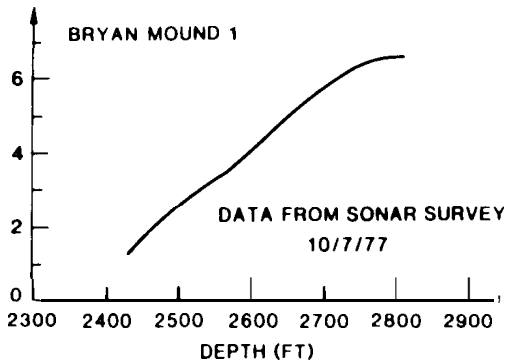

c CAVERN VOLUME DATA

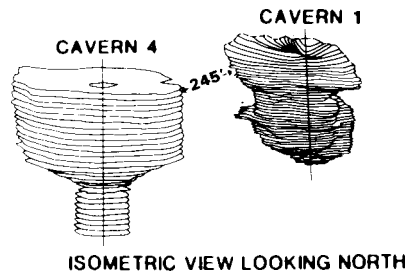

d CAVERN SEPARATION DISTANCE (SEC. II)

Figure 14. Bryan Mound Cavern One

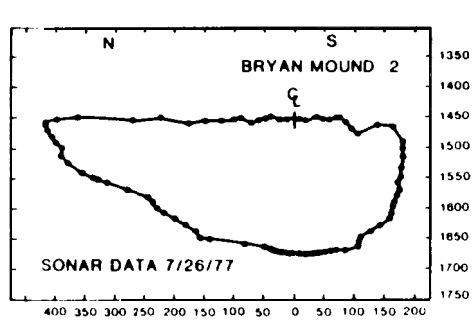

a. SONAR PROFILE

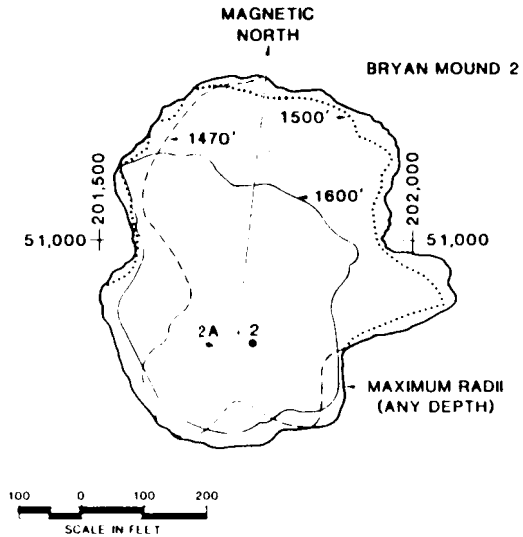

b. HORIZONTAL PROFILES (SEC. II)

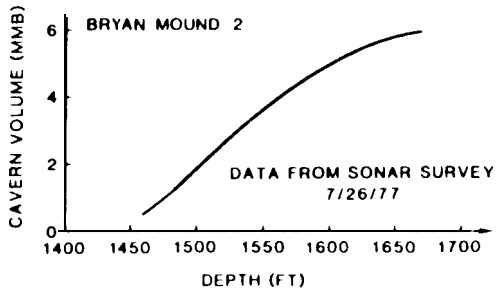

c. CAVERN VOLUME DATA

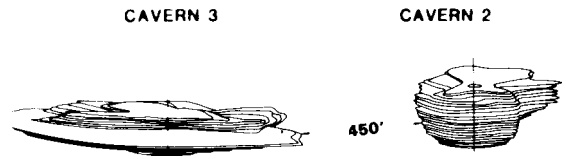

ISOMETRIC VIEW LOOKING NORTH

d. CAVERN SEPARATION DISTANCE (SEC. II)

Figure 15: Bryan Mound Cavern Two.

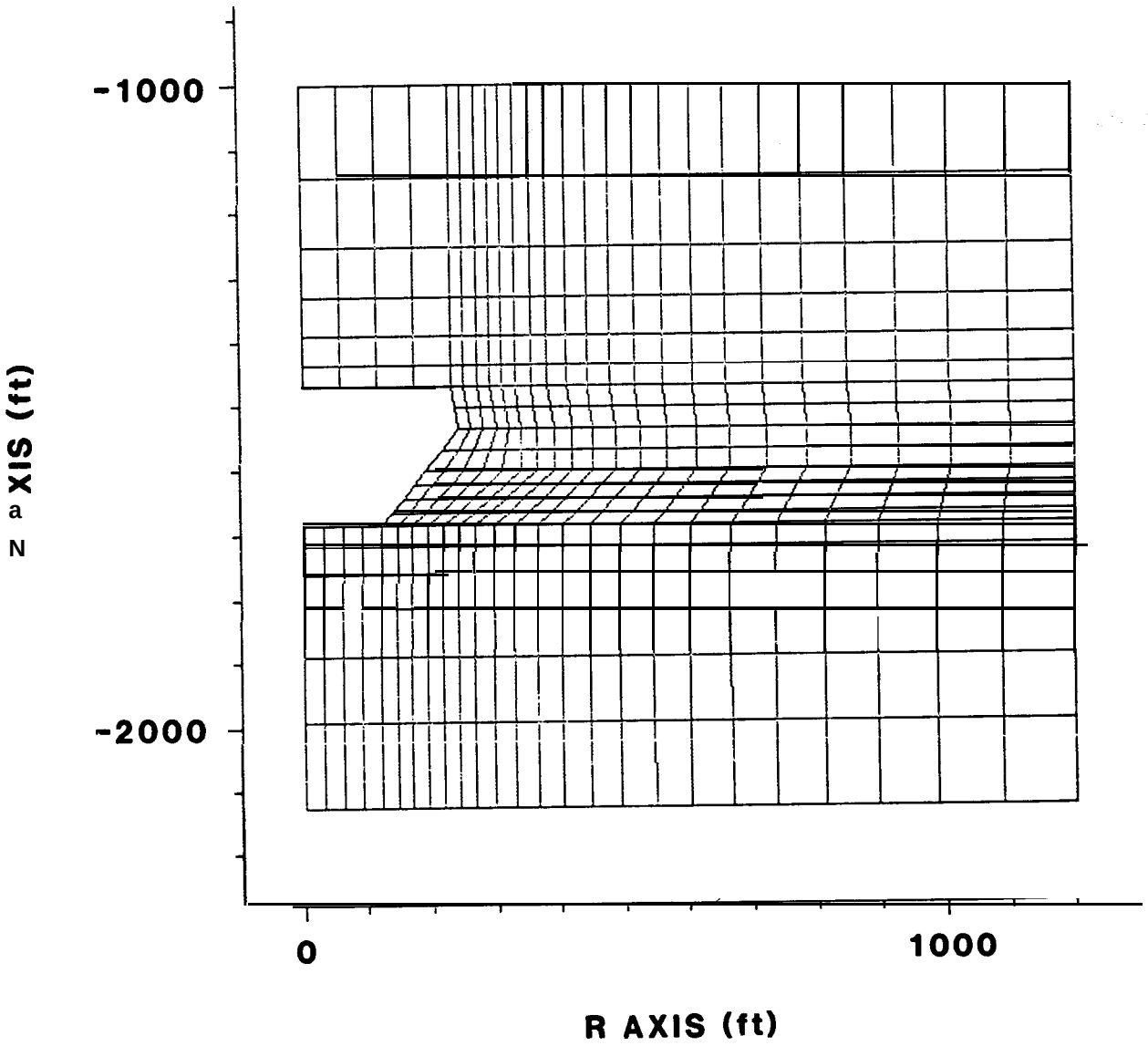

Figure -16. Axisymmetric Finite Element Model of Bryan Mound Cavern Two.

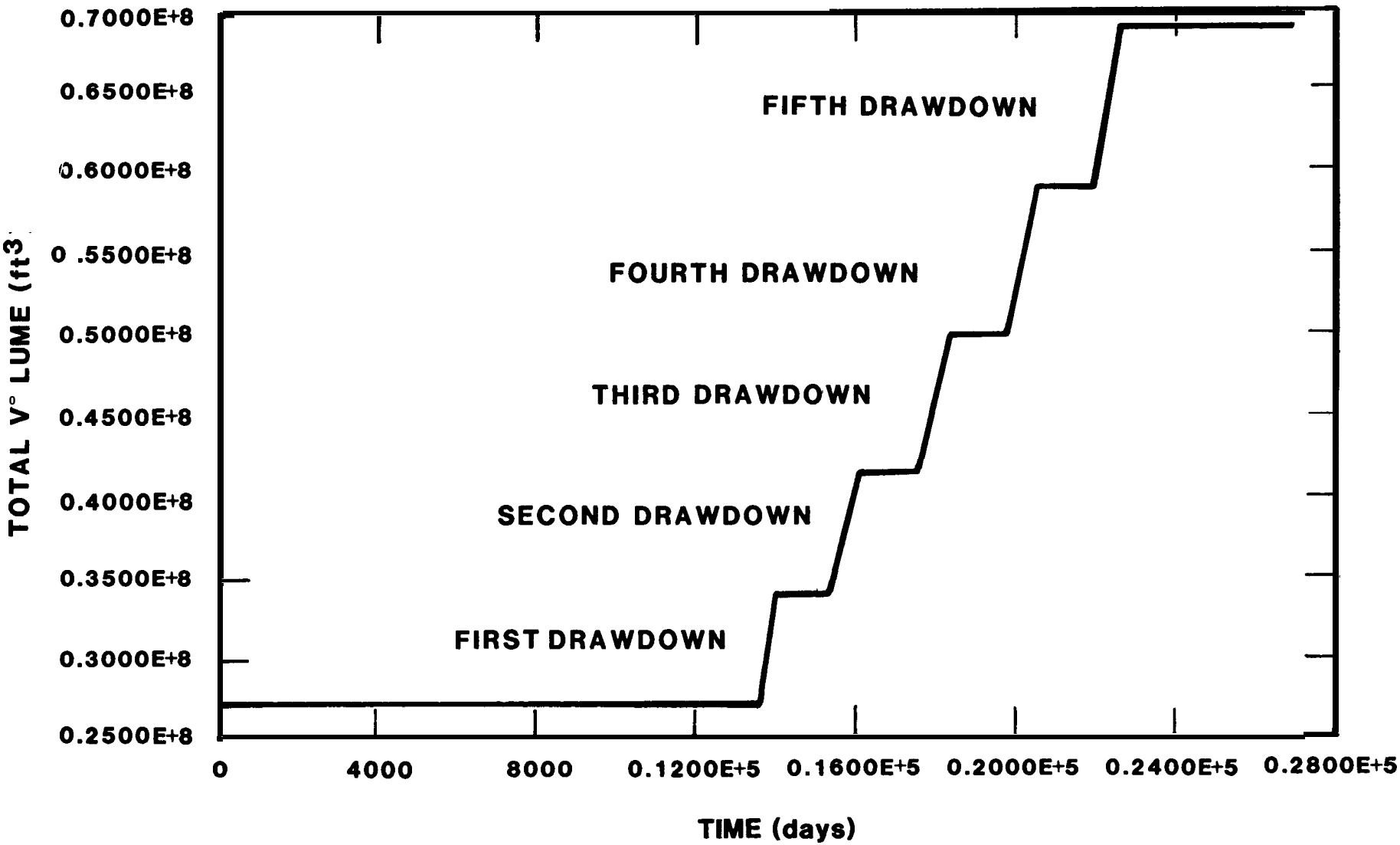

Figure 17. Volumetric Response of Bryan Mound Cavern Two.

SONAR DATA 10/23/79

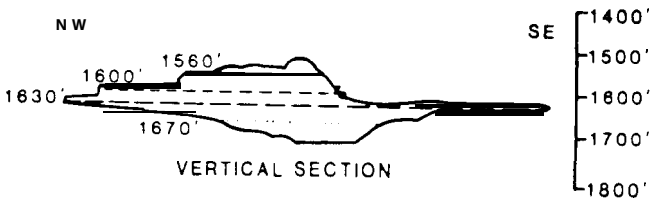

a. SONAR PROFILE (SEC. II)

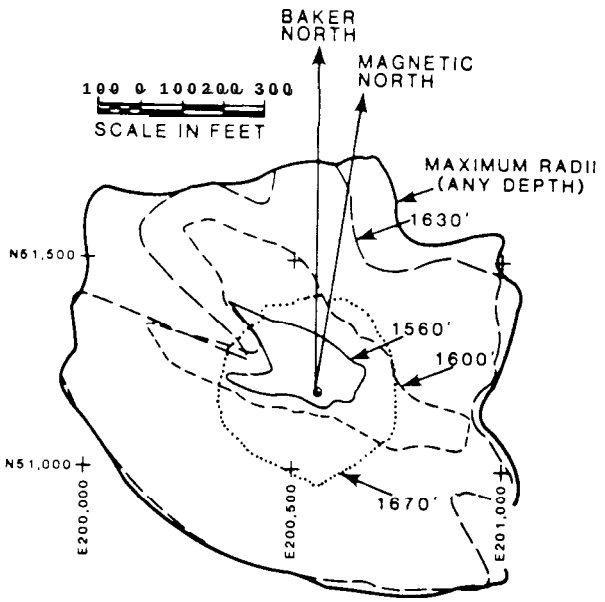

b. HORIZONTAL SECTIONS (SEC. II)

Figure 18: Bryan Mound Cavern Three

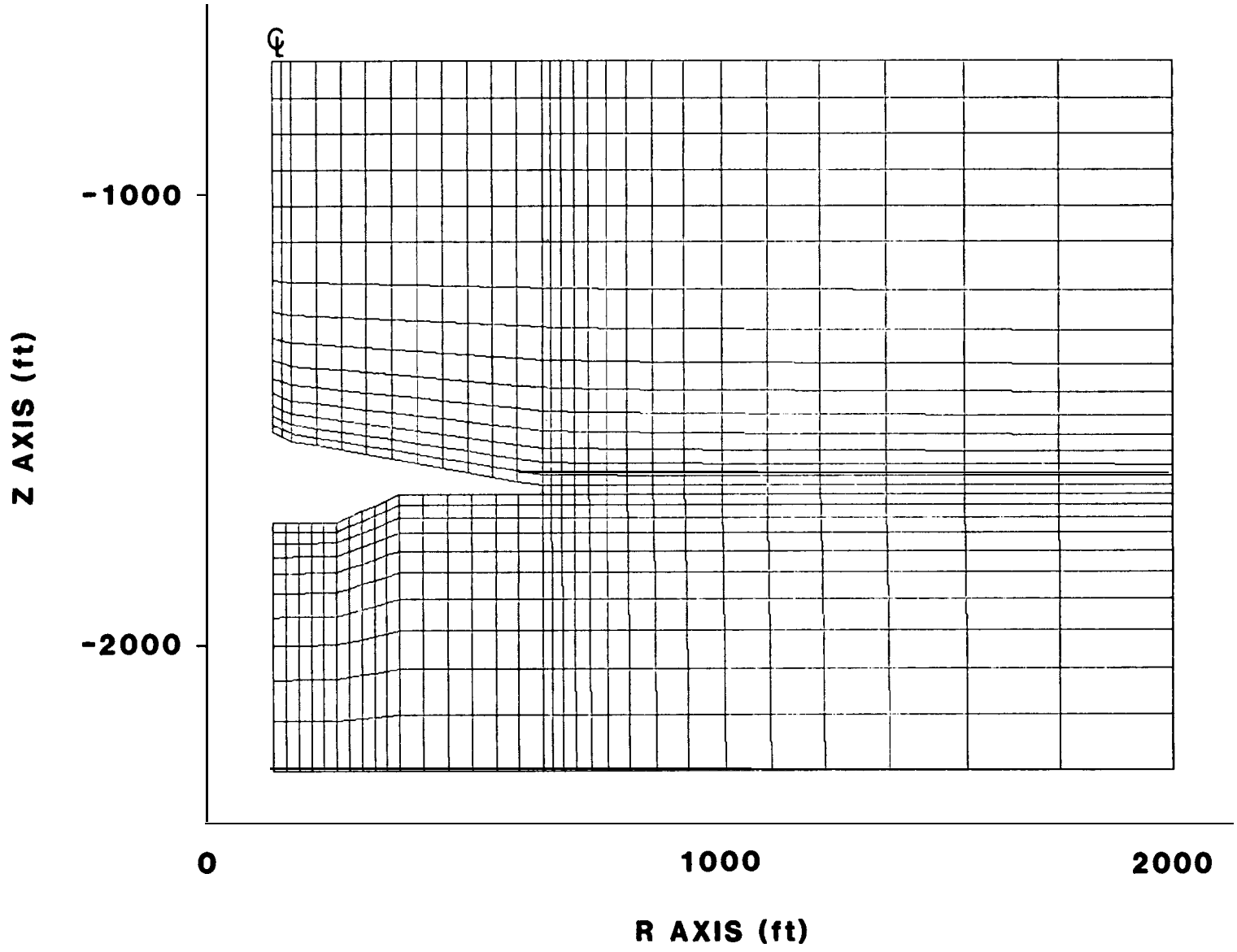

Figure 19: Axisymmetric Finite Element Model of Bryan Mound Cavern Three.

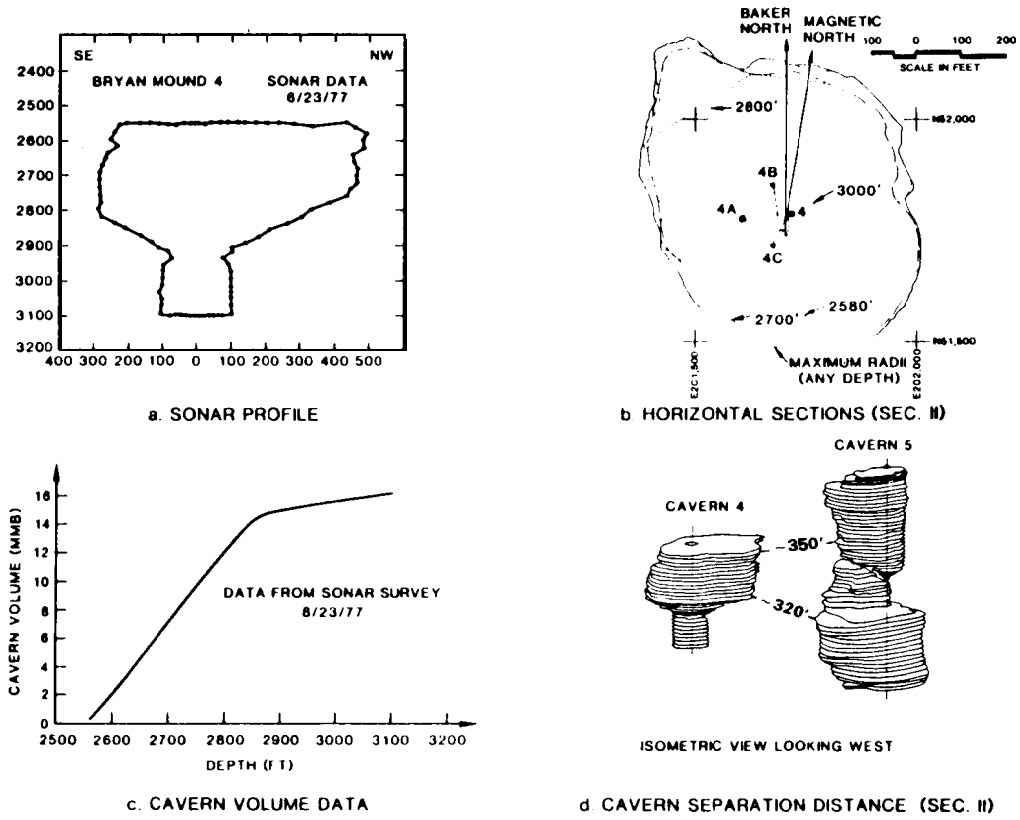

Figure 20: Bryan Mound Cavern Four.

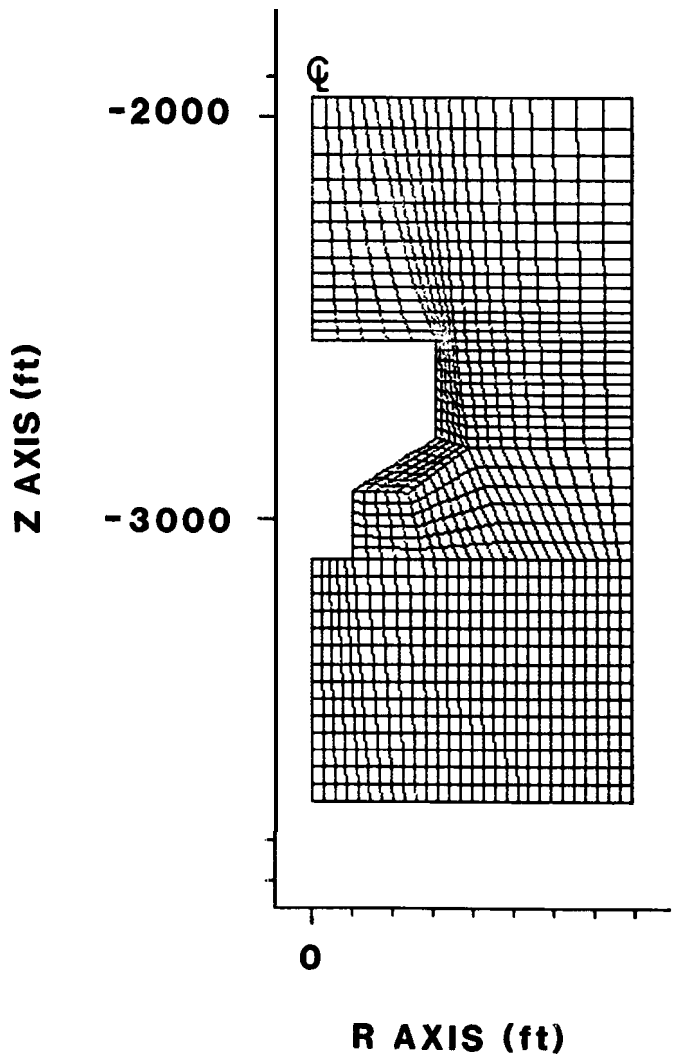

Figure 21. Axisymmetric Finite Element Model of Bryan Mound Cavern Four.

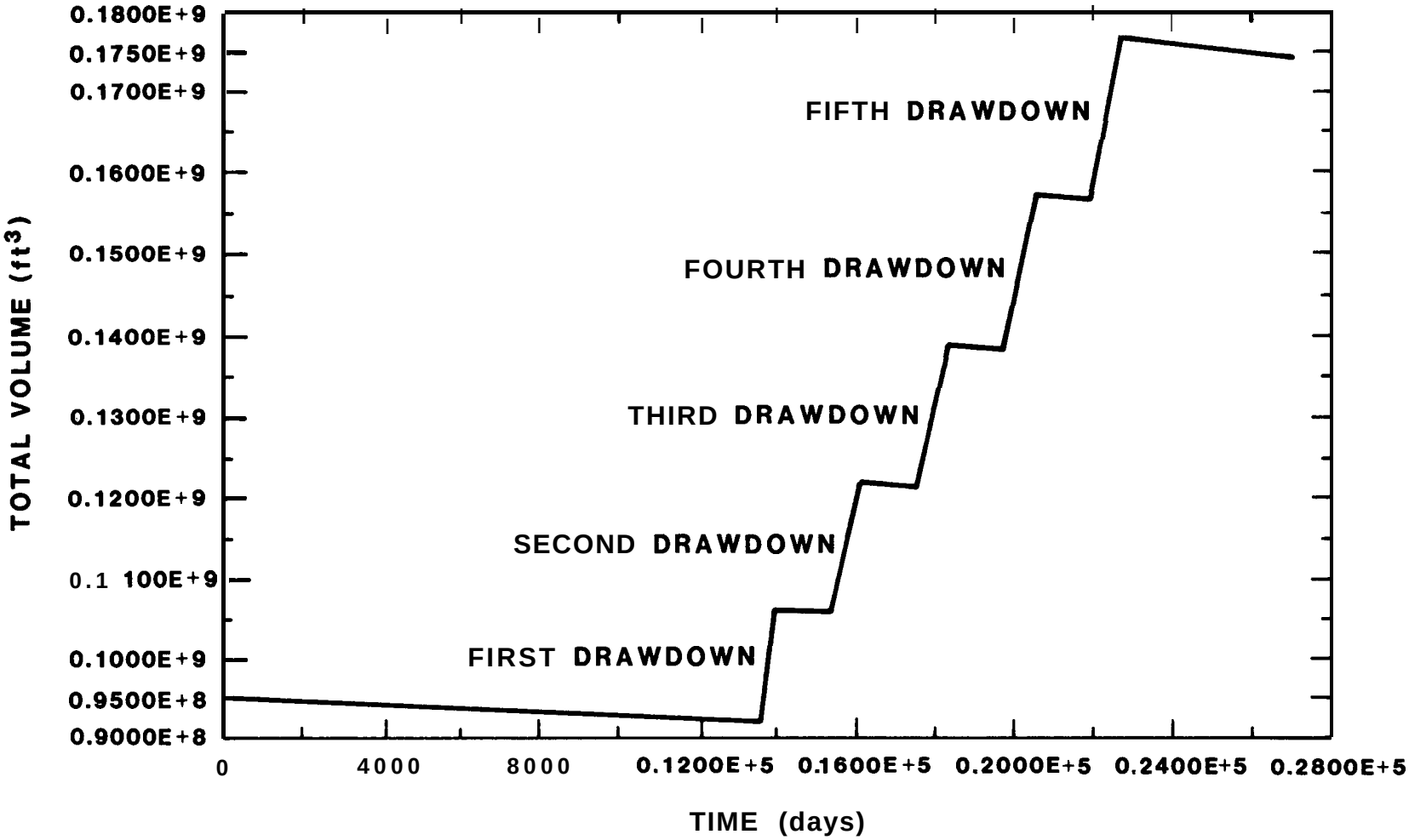

Figure 22. Volumetric Response of Bryan Mound Cavern Four.

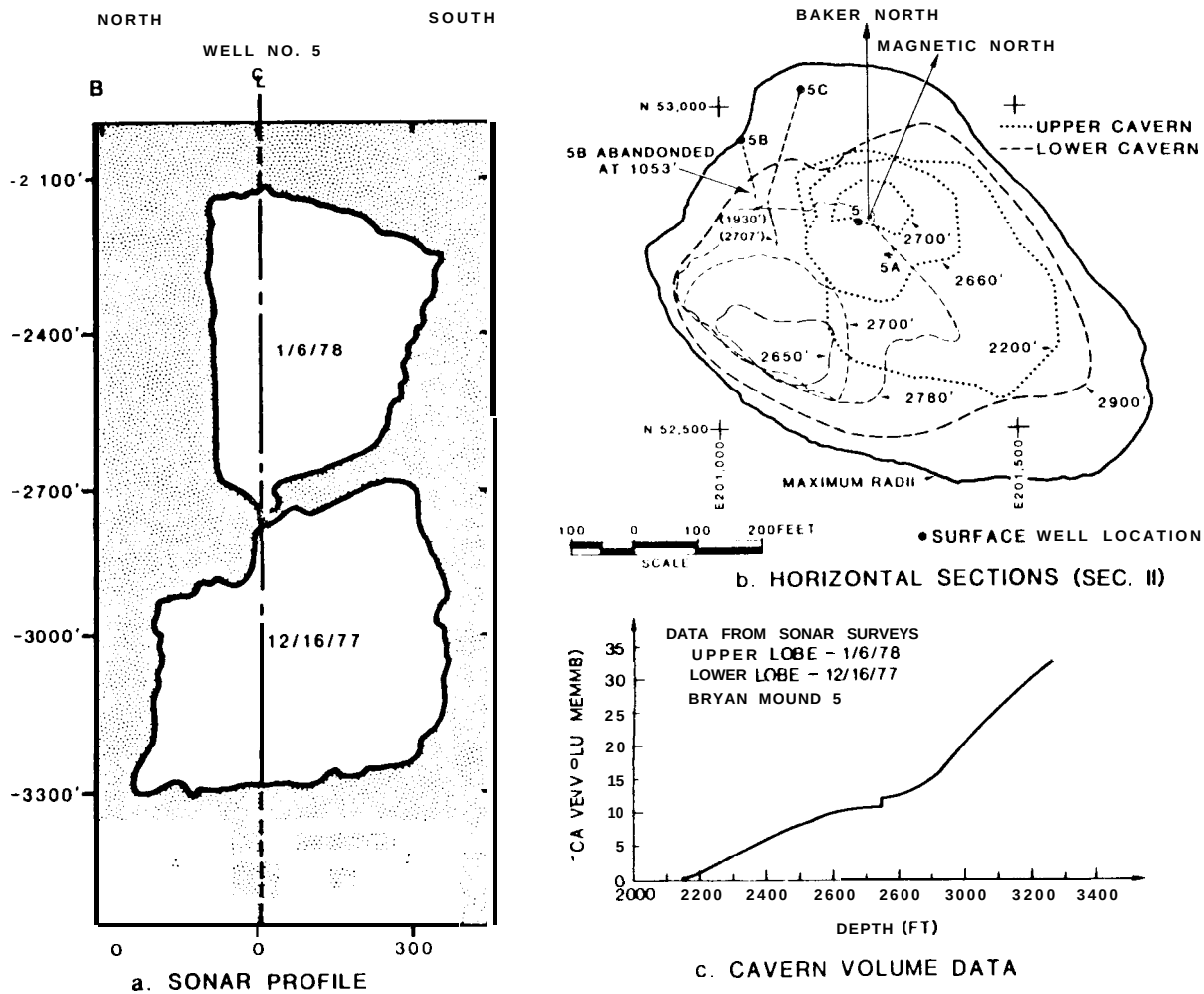

Figure 23. Bryan Mound Cavern Five

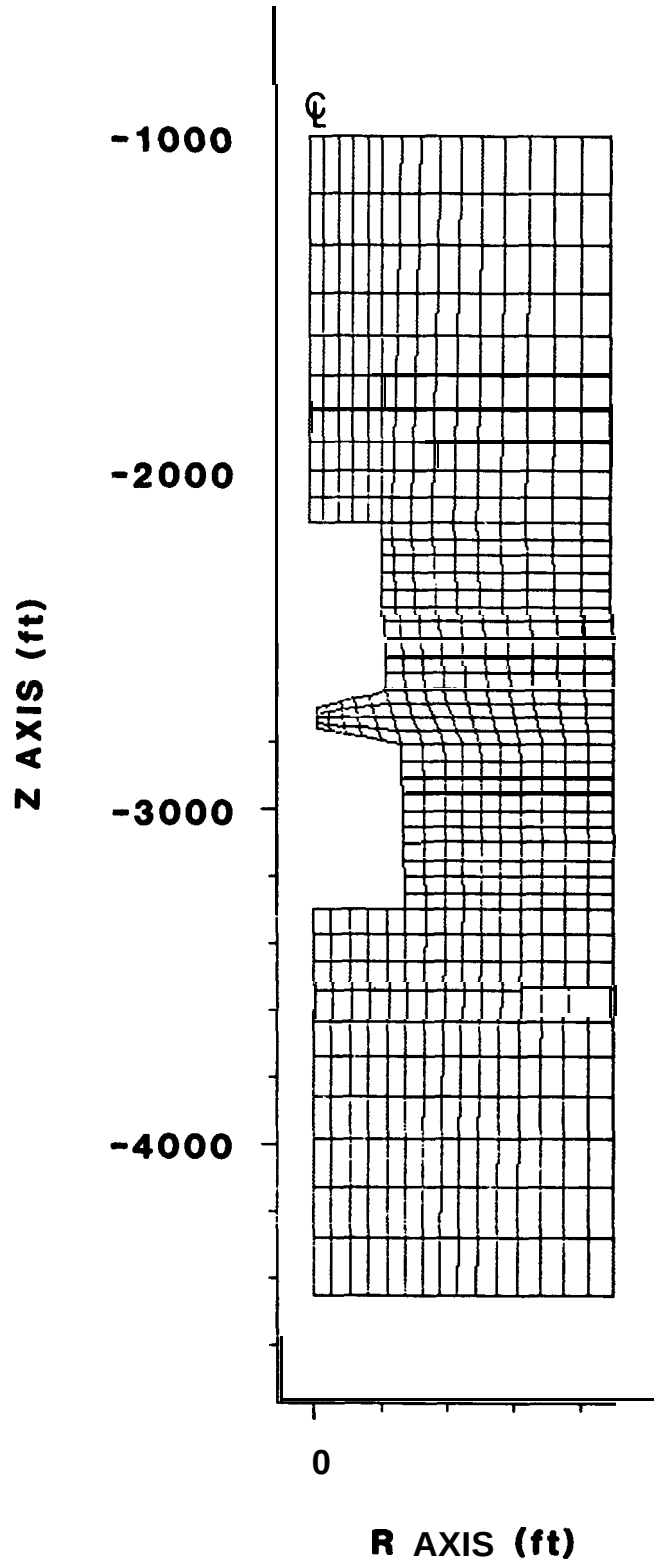

Figure 24. Axisymmetric Finite Element Model of Bryan Mound Cavern Five.

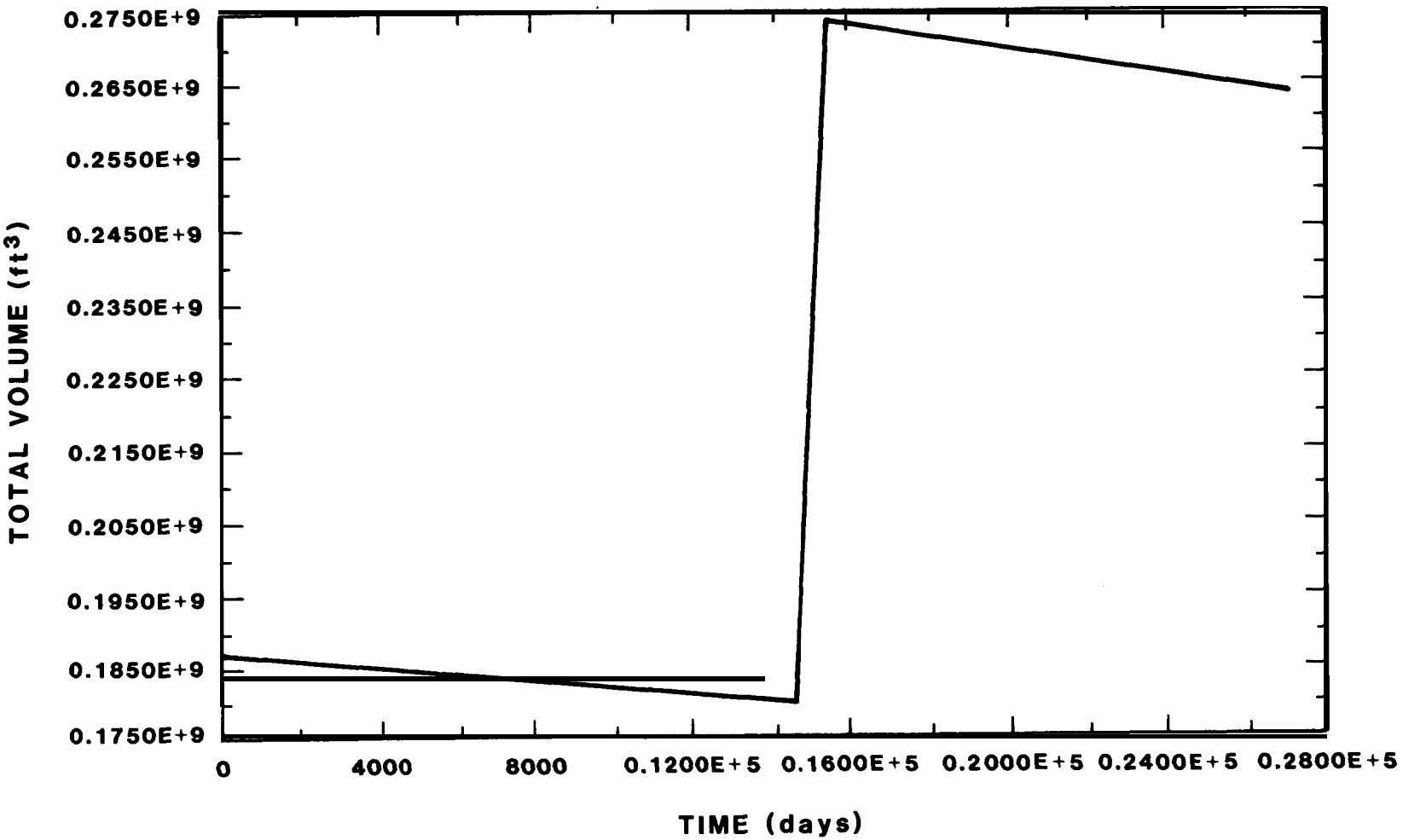

Figure 25. Volumetric Response of Bryan Mound Cavern Five

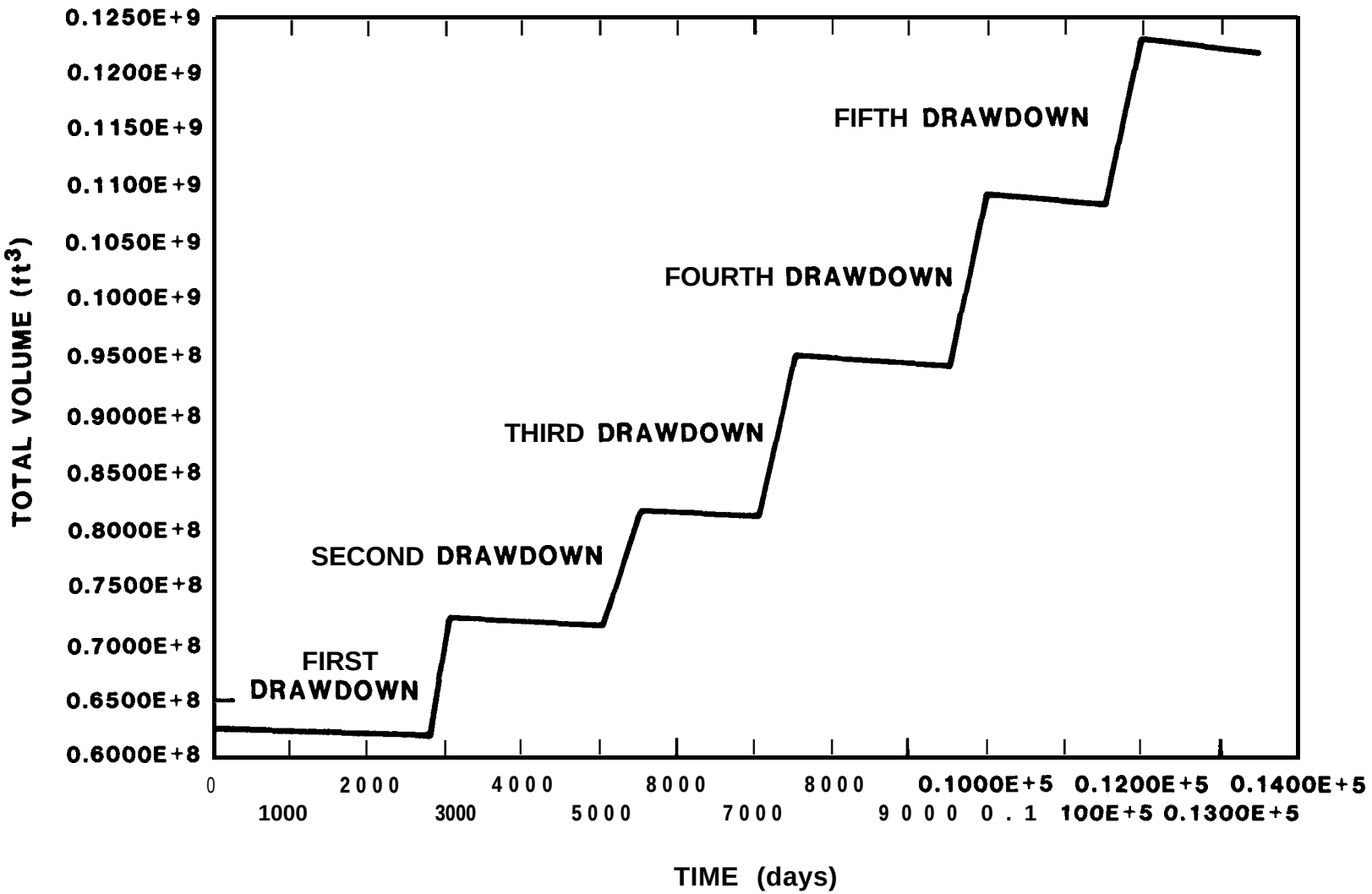

Figure 26. Volumetric Response of Bryan Mound Expansion Caverns.

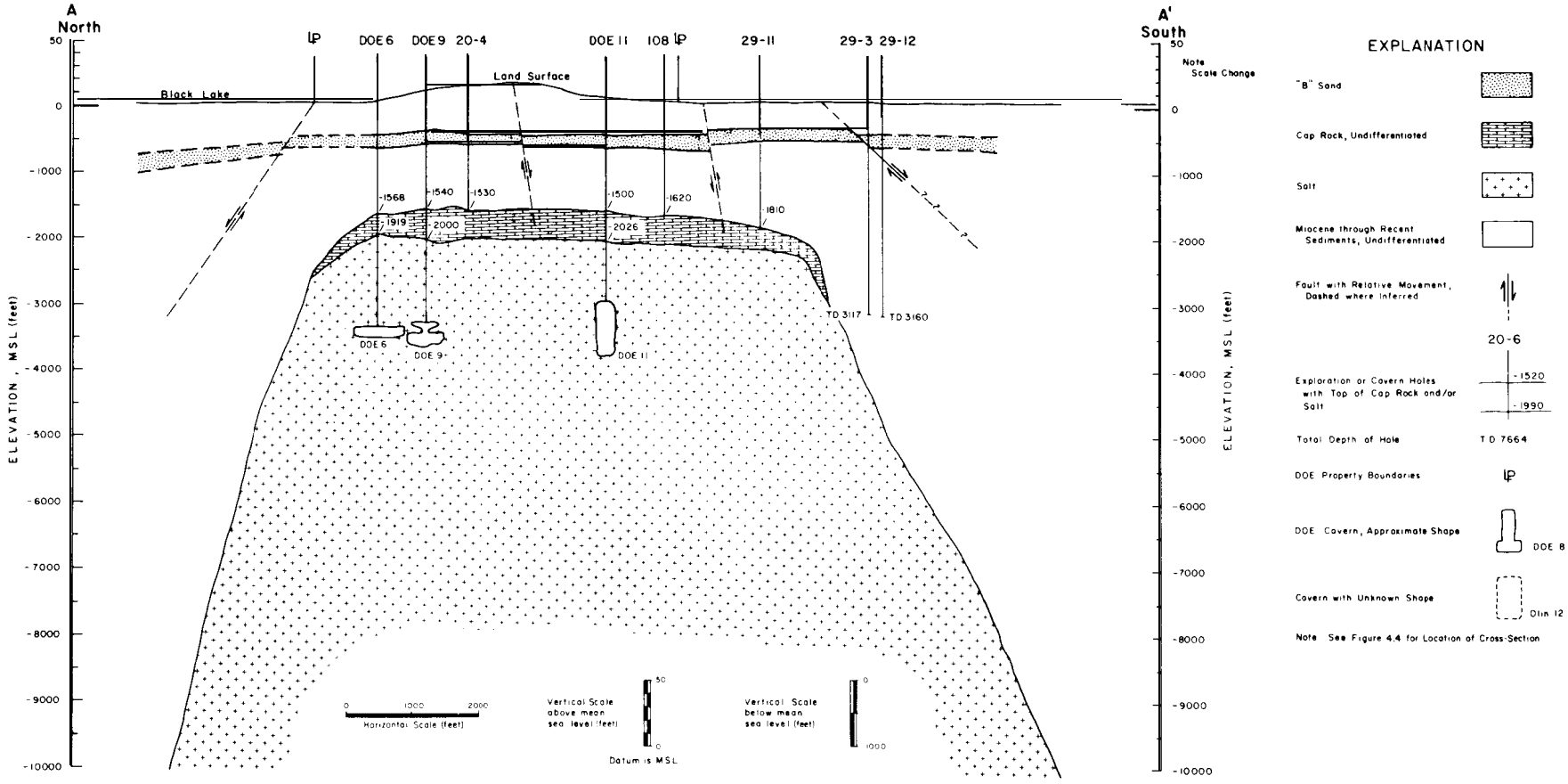

Figure 27 Cross-Section of West Hackberry Salt Dome.

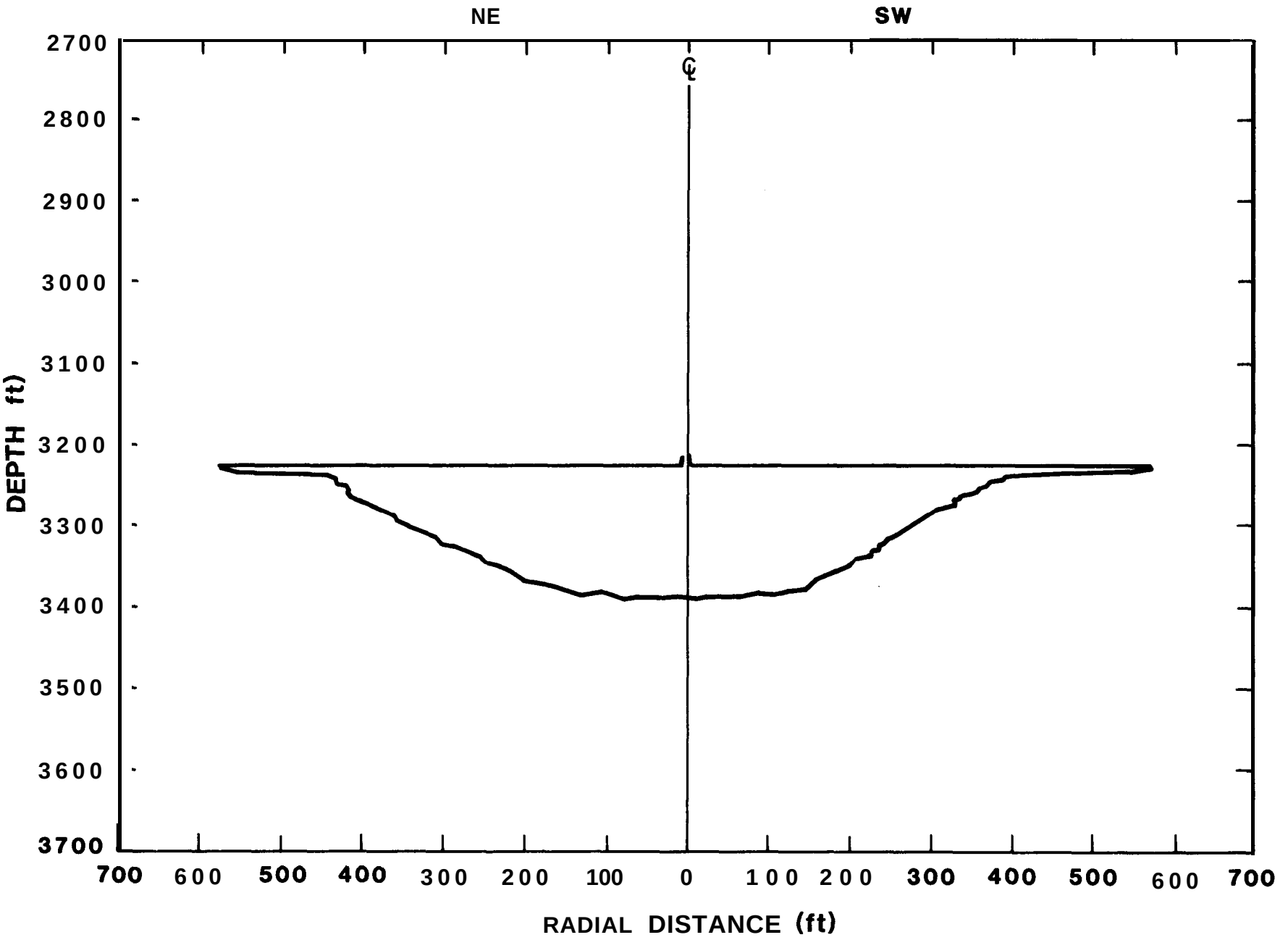

Figure 28. West Hackberry Cavern Six.

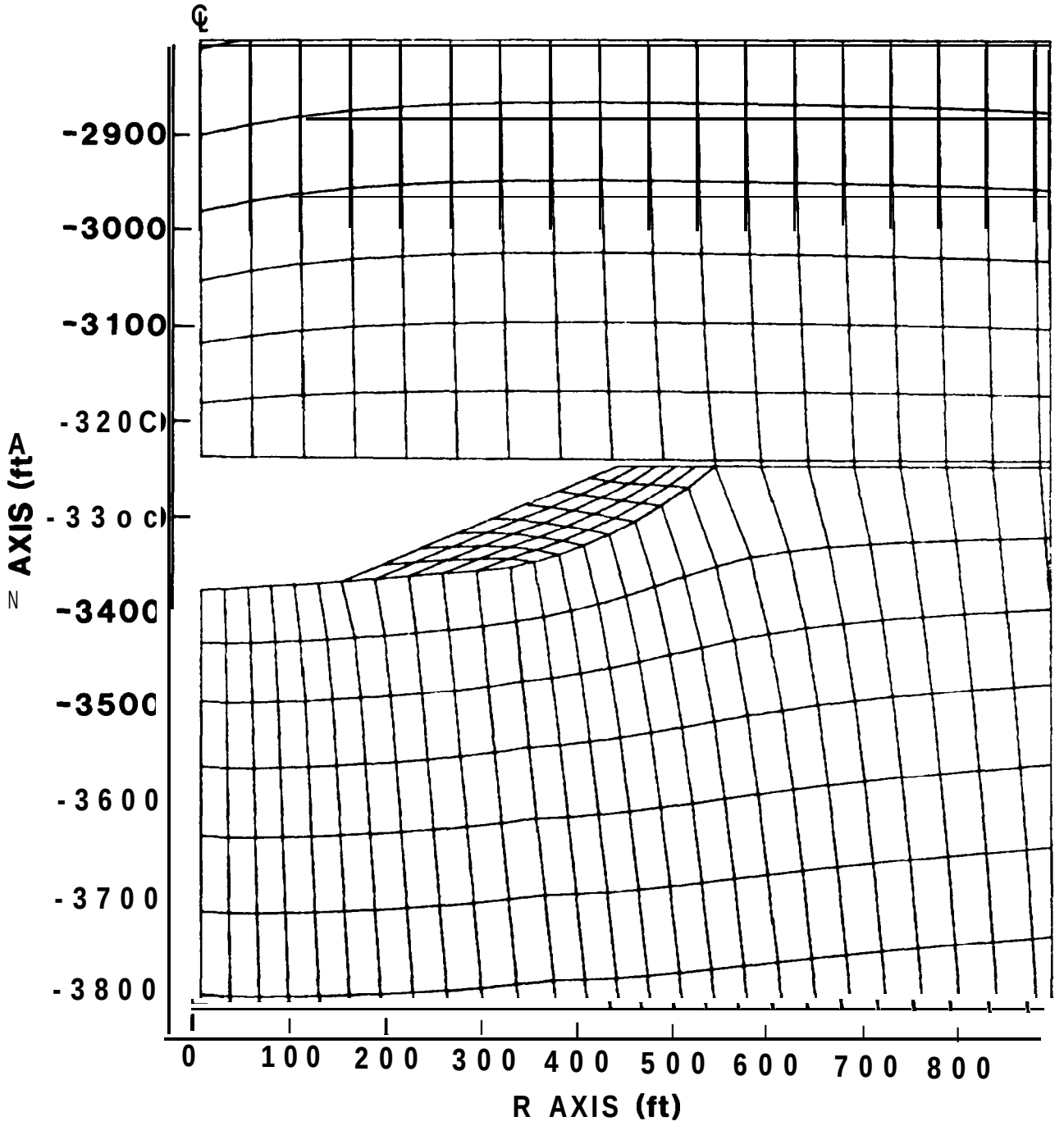

Figure 29. Close-Up of Axisymmetric Finite Element Model of West Hackberry Cavern Six.

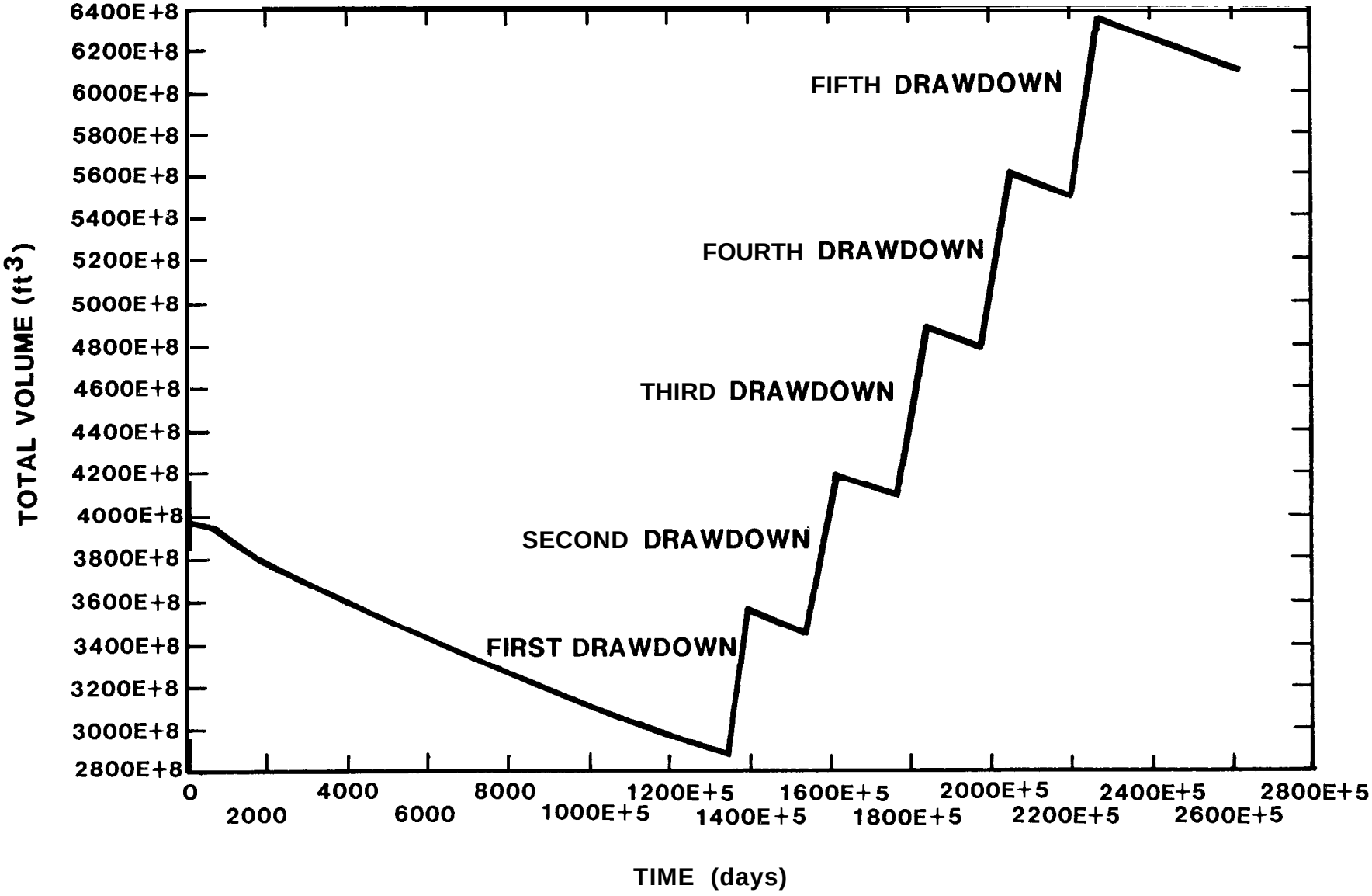

Figure 30. Volumetric Response of West Hackberry Cavern Six

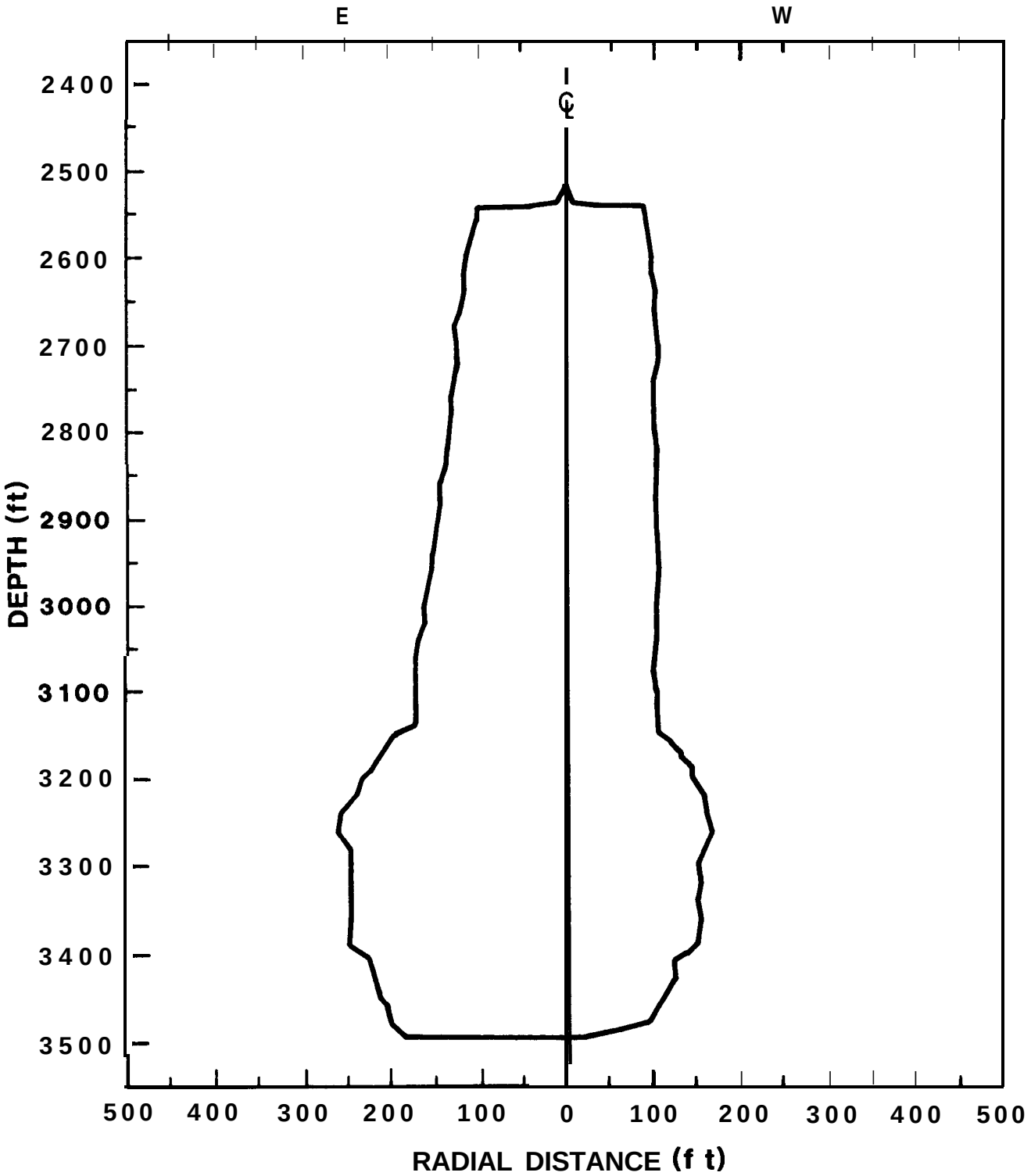

Figure 31. West Hackberry Cavern Seven.

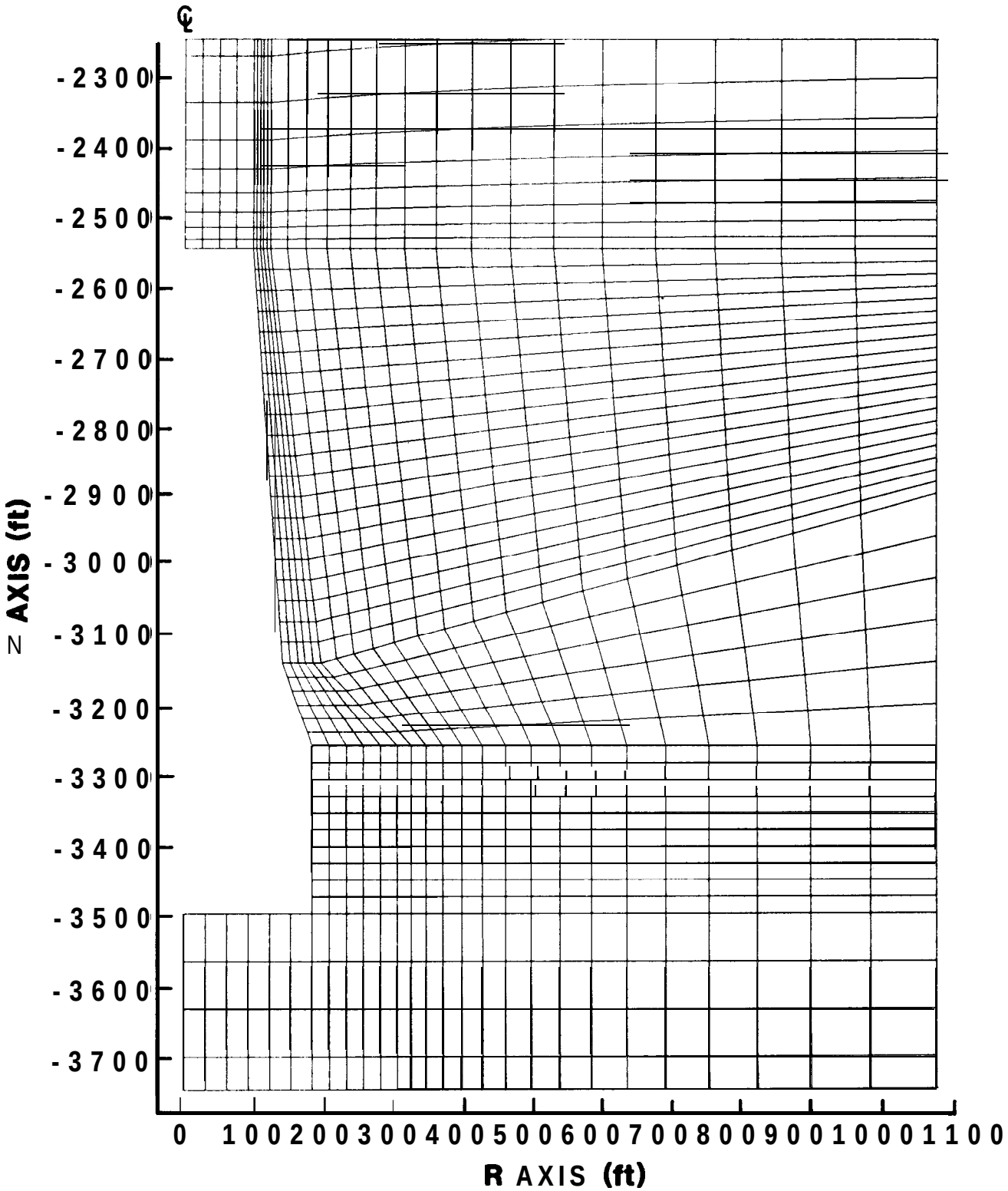

Figure 32. Close-Up of Axisymmetric Finite Element Model of West Hackberry Cavern Seven.

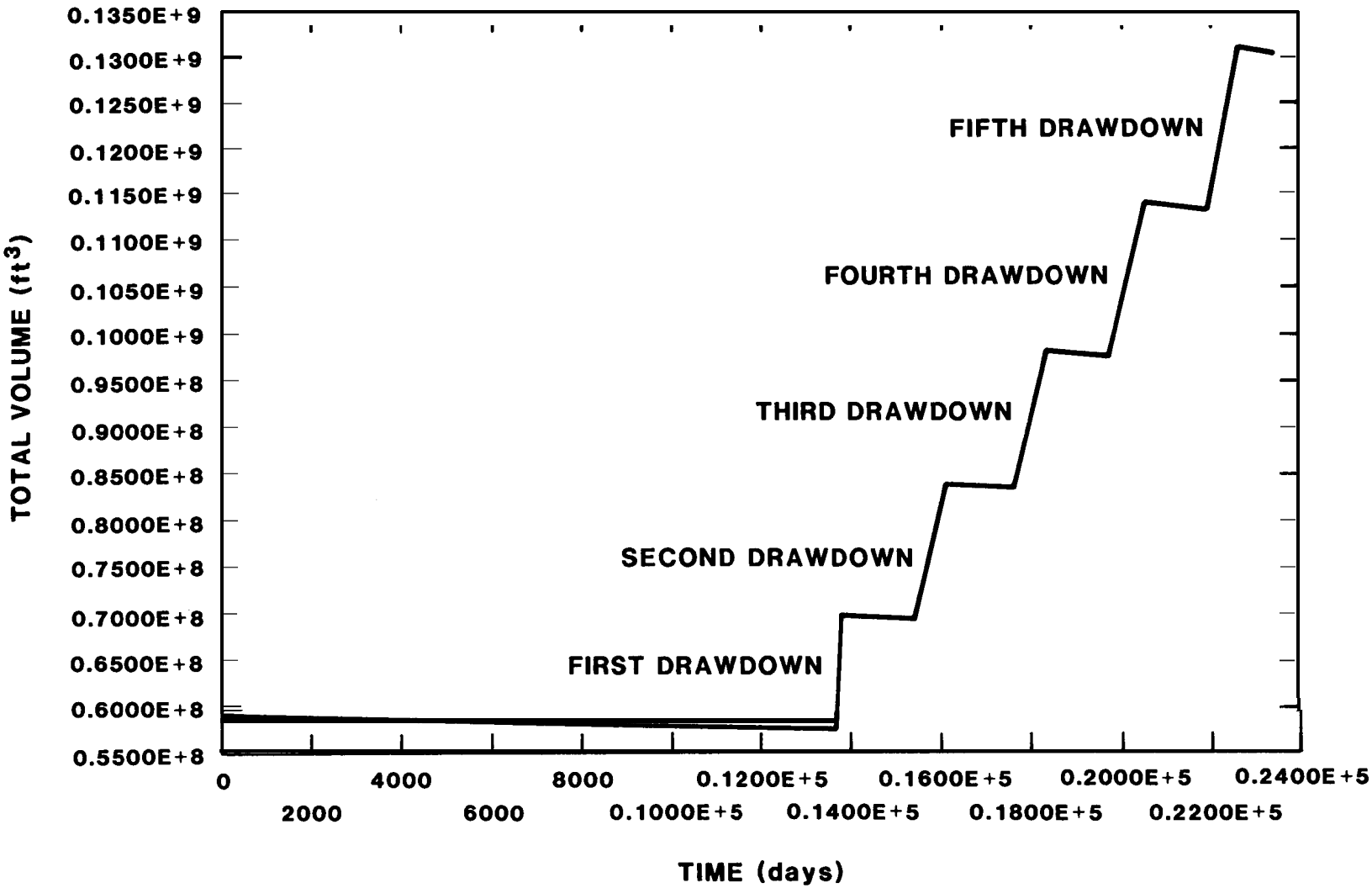

Figure 33. Volumetric Response of West Hackberry Cavern Seven.

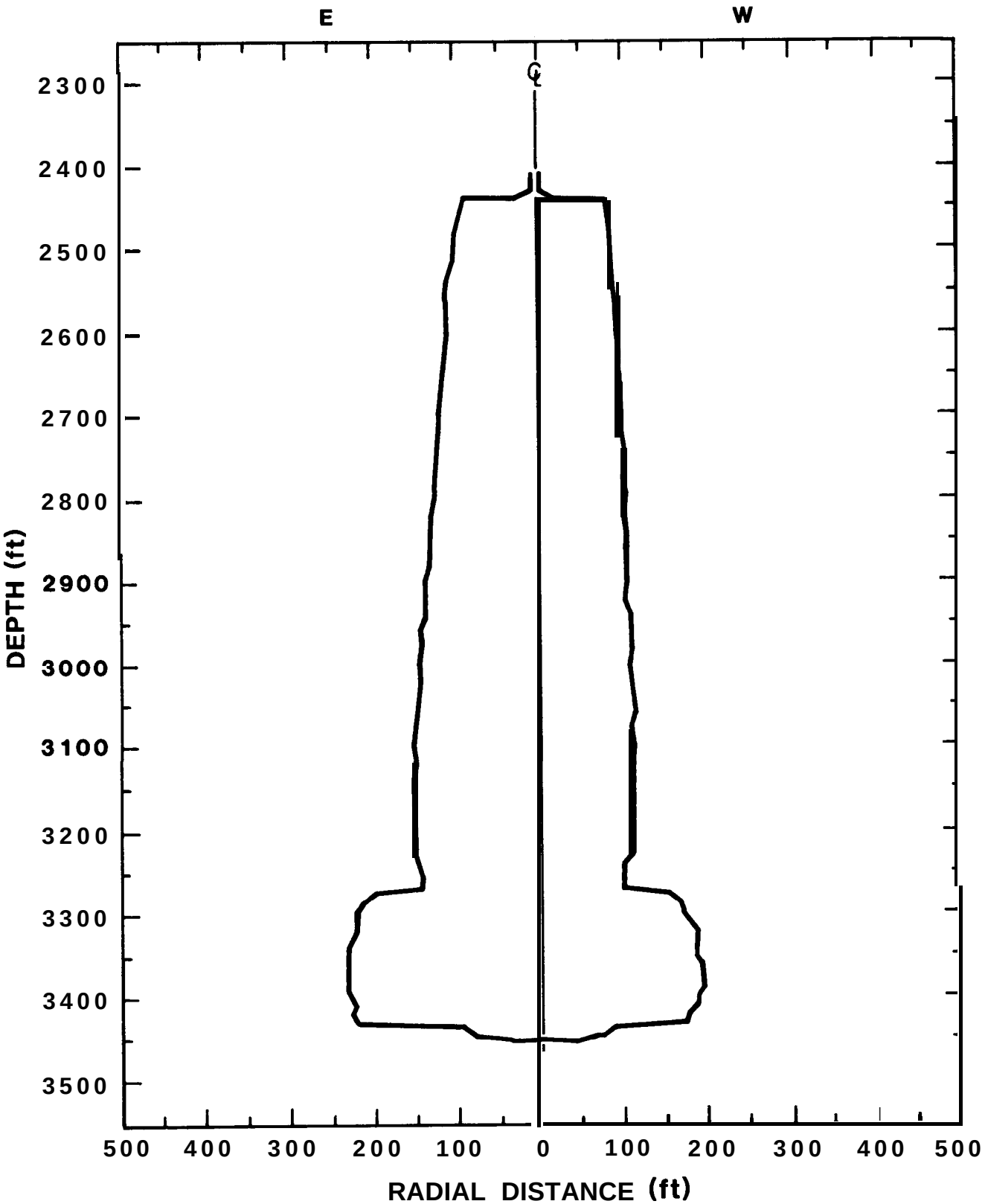

Figure 34. West Hackberry Cavern Eight.

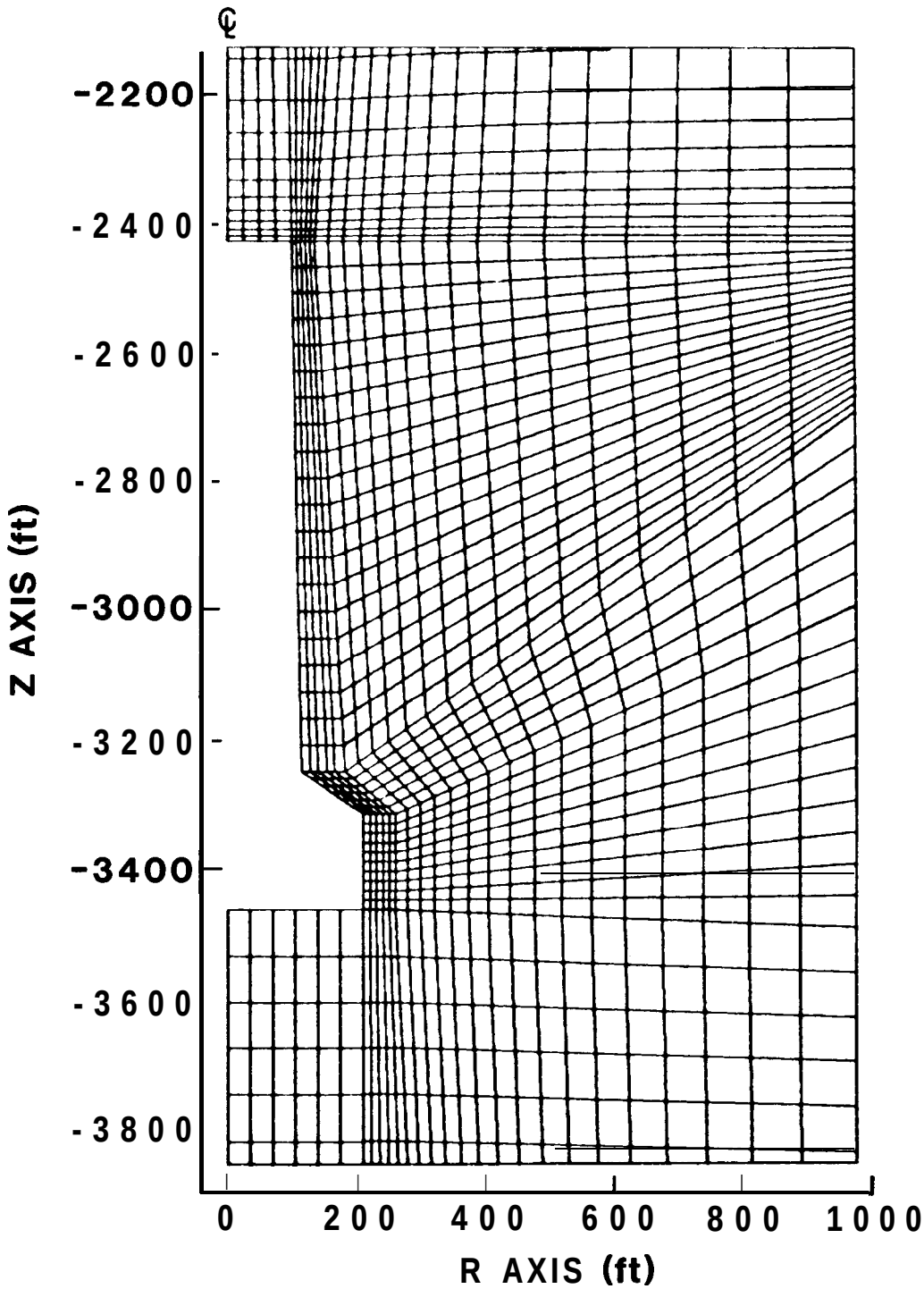

Figure 35. Close-Up of Axisymmetric Finite Element Model of West Hackberry Cavern Eight.

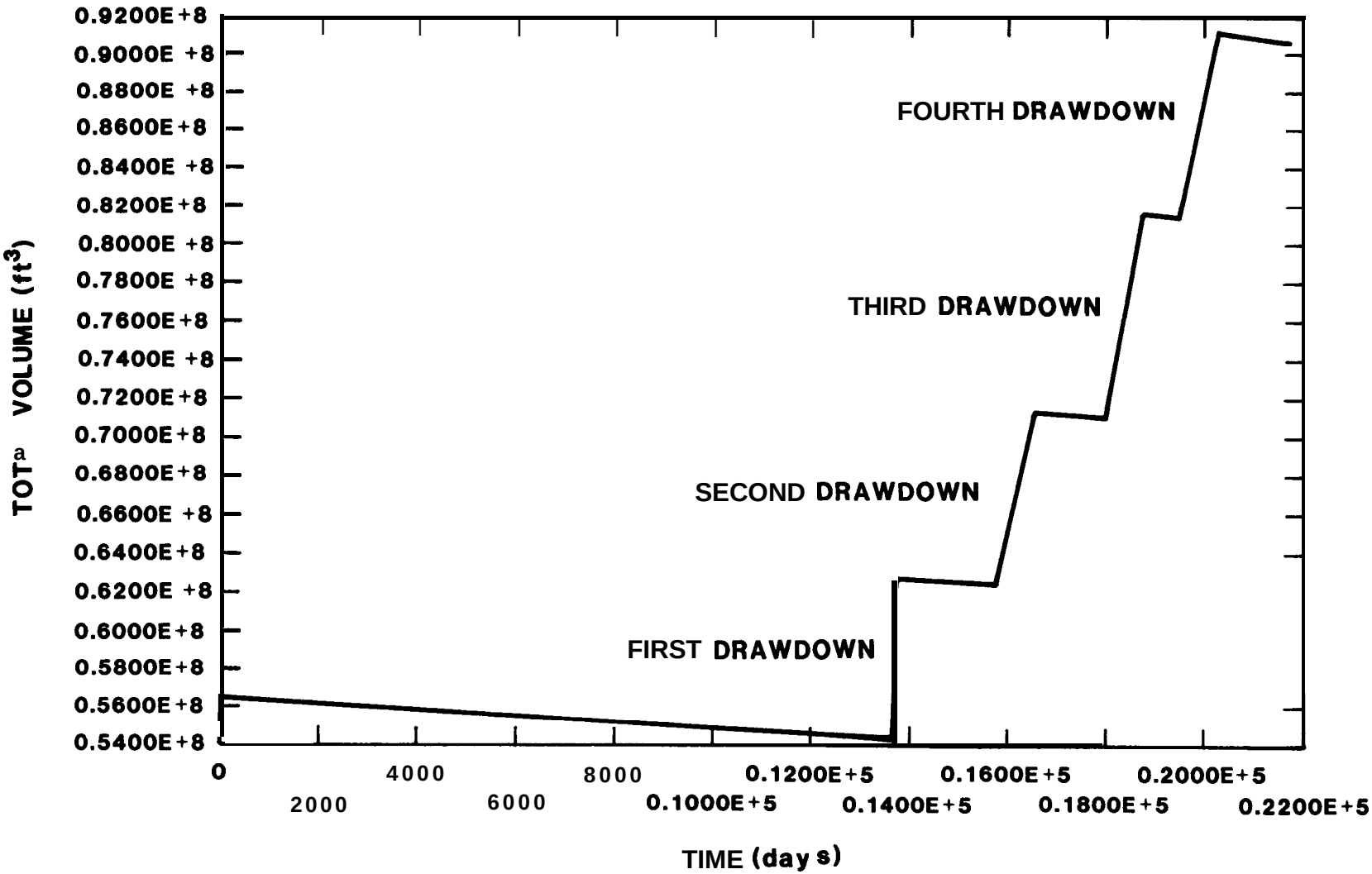

Figure 36. Volumetric Response of West Hackberry Cavern Eight.

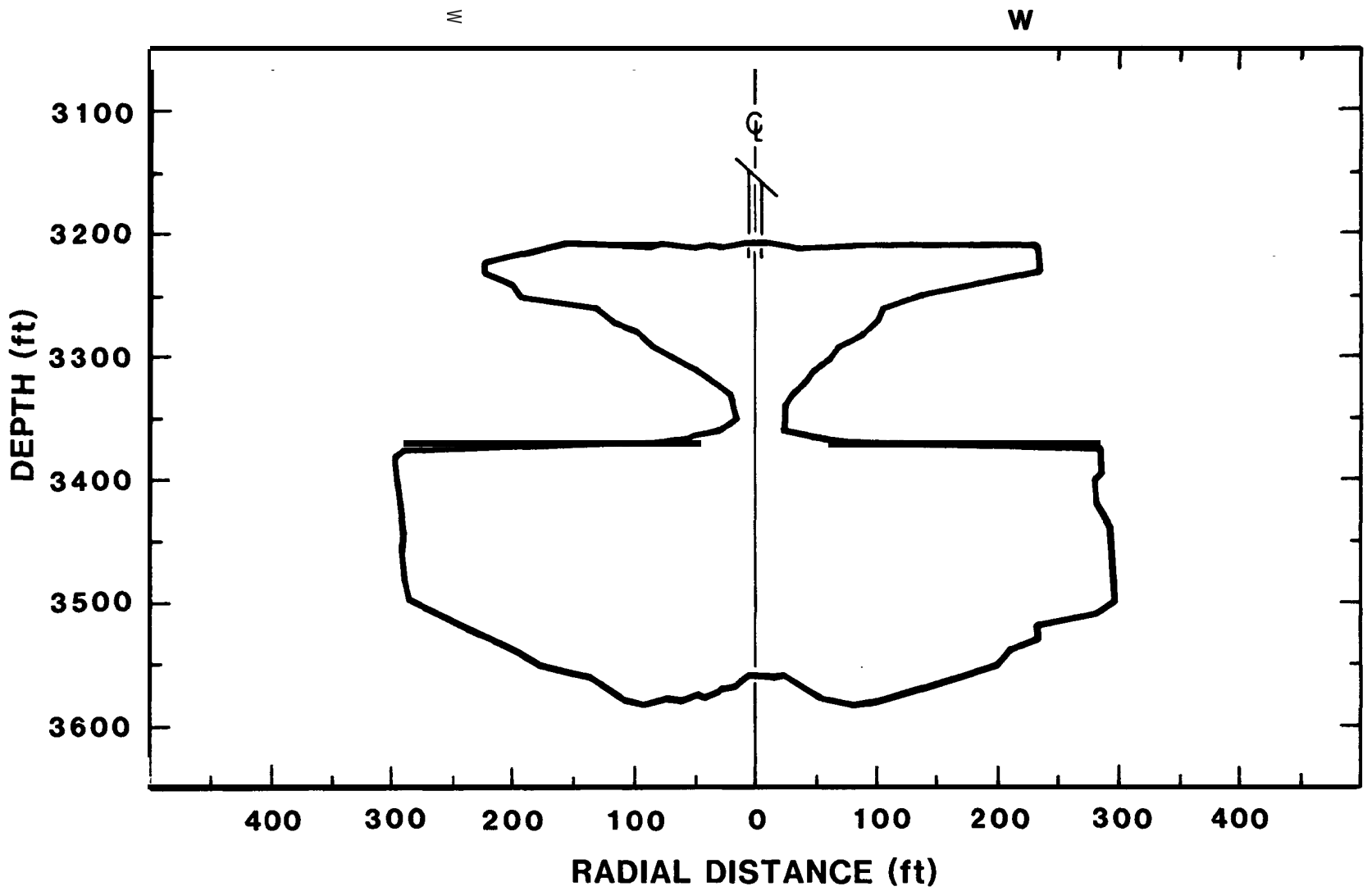

Figure 37. West Hackberry Cavern Nine.

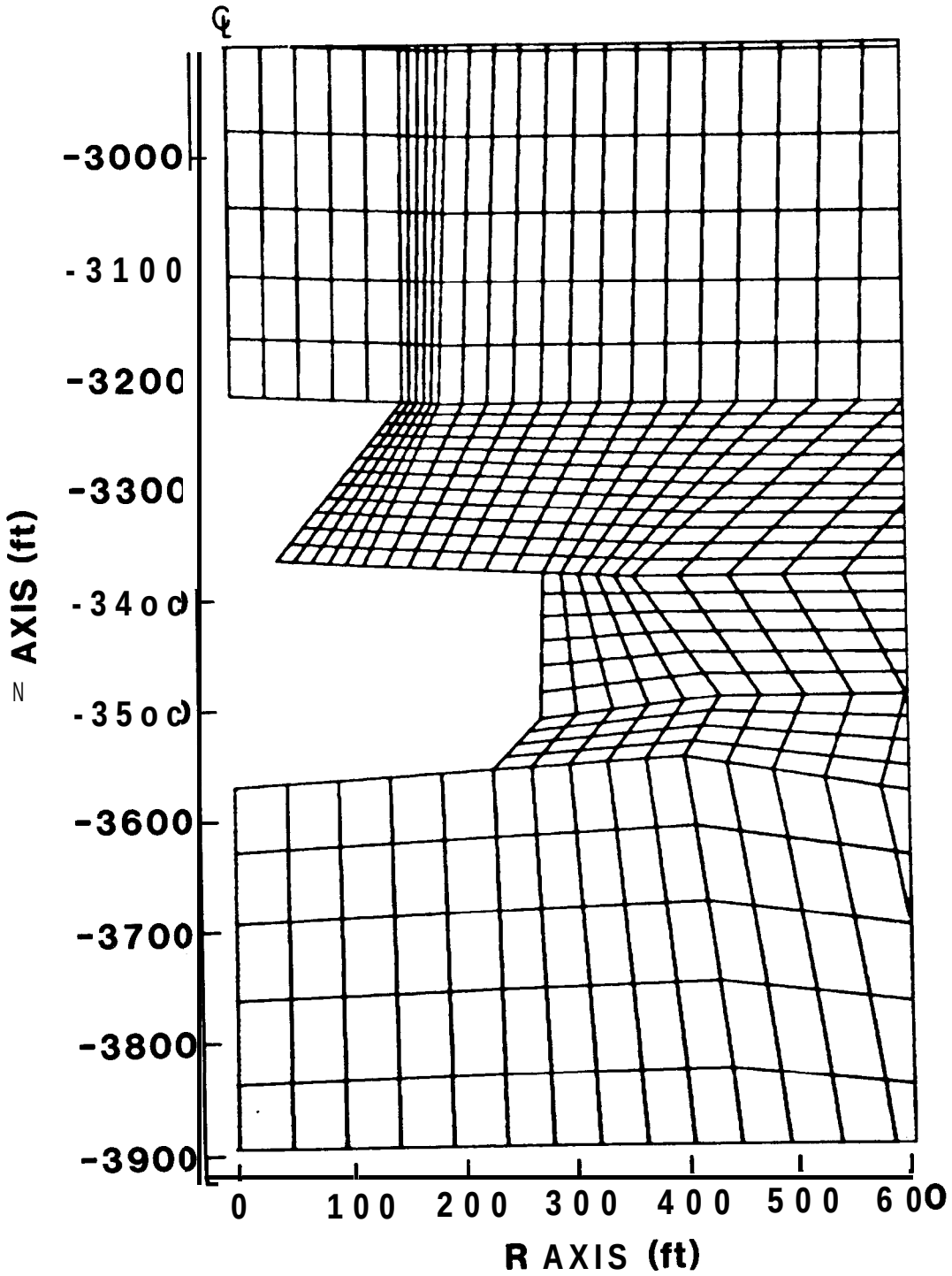

Figure 38. Close-Up of Axisymmetric Finite Element Model of West Hackberry Cavern Nine.

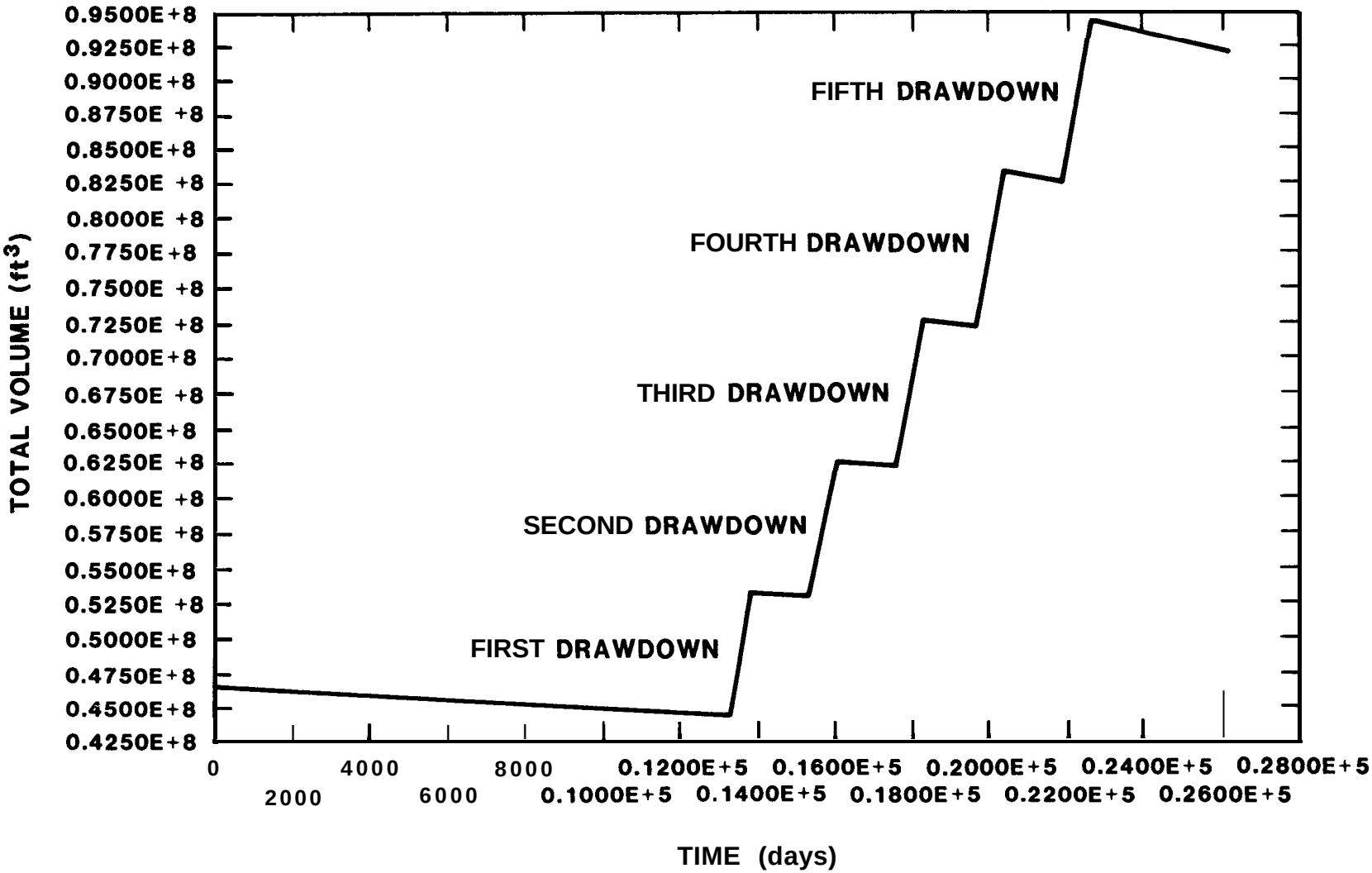

Figure 39. Volumetric Response of West Hackberry Cavern Nine.

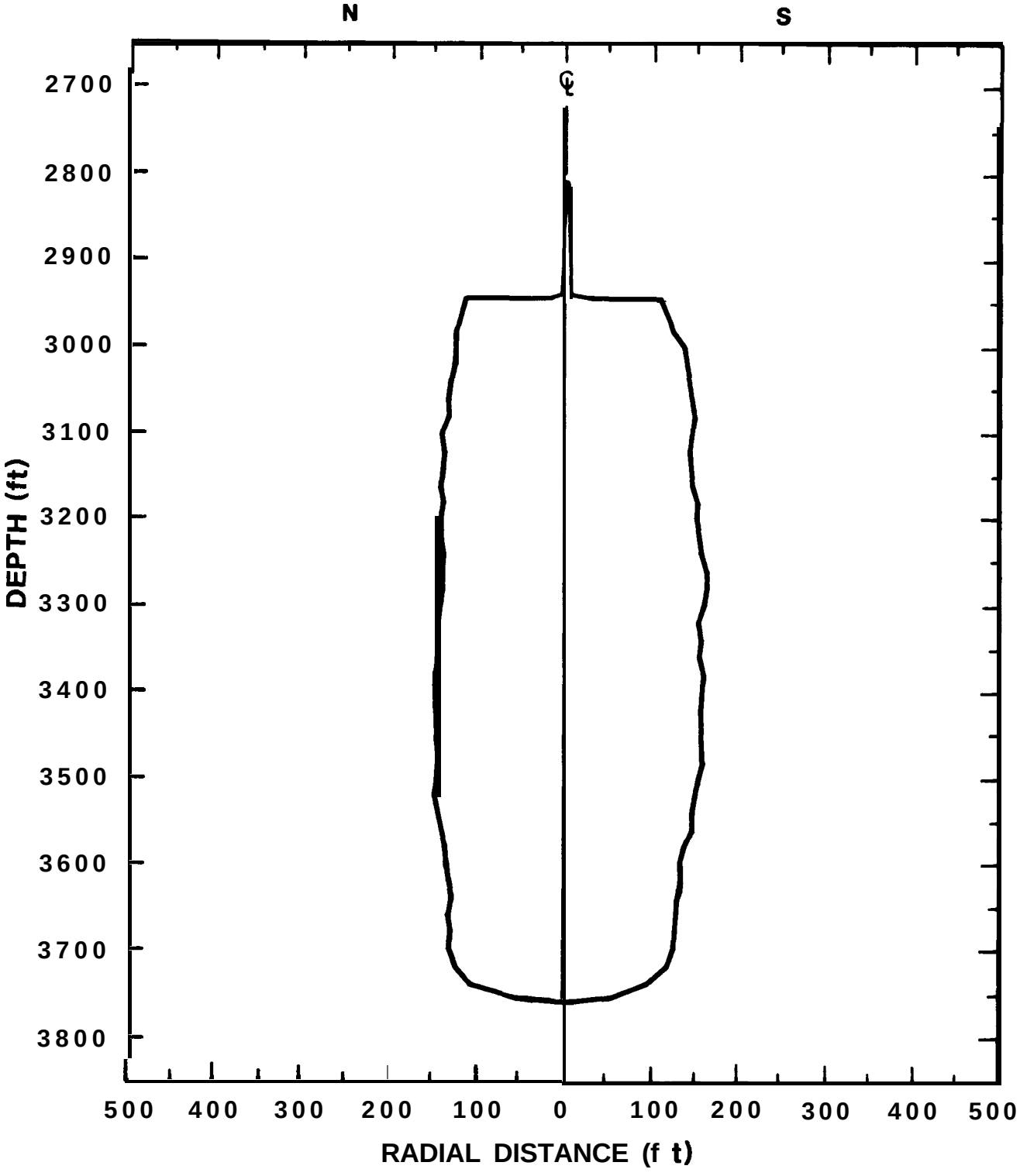

Figure 40. West Hackberry Cavern Eleven.

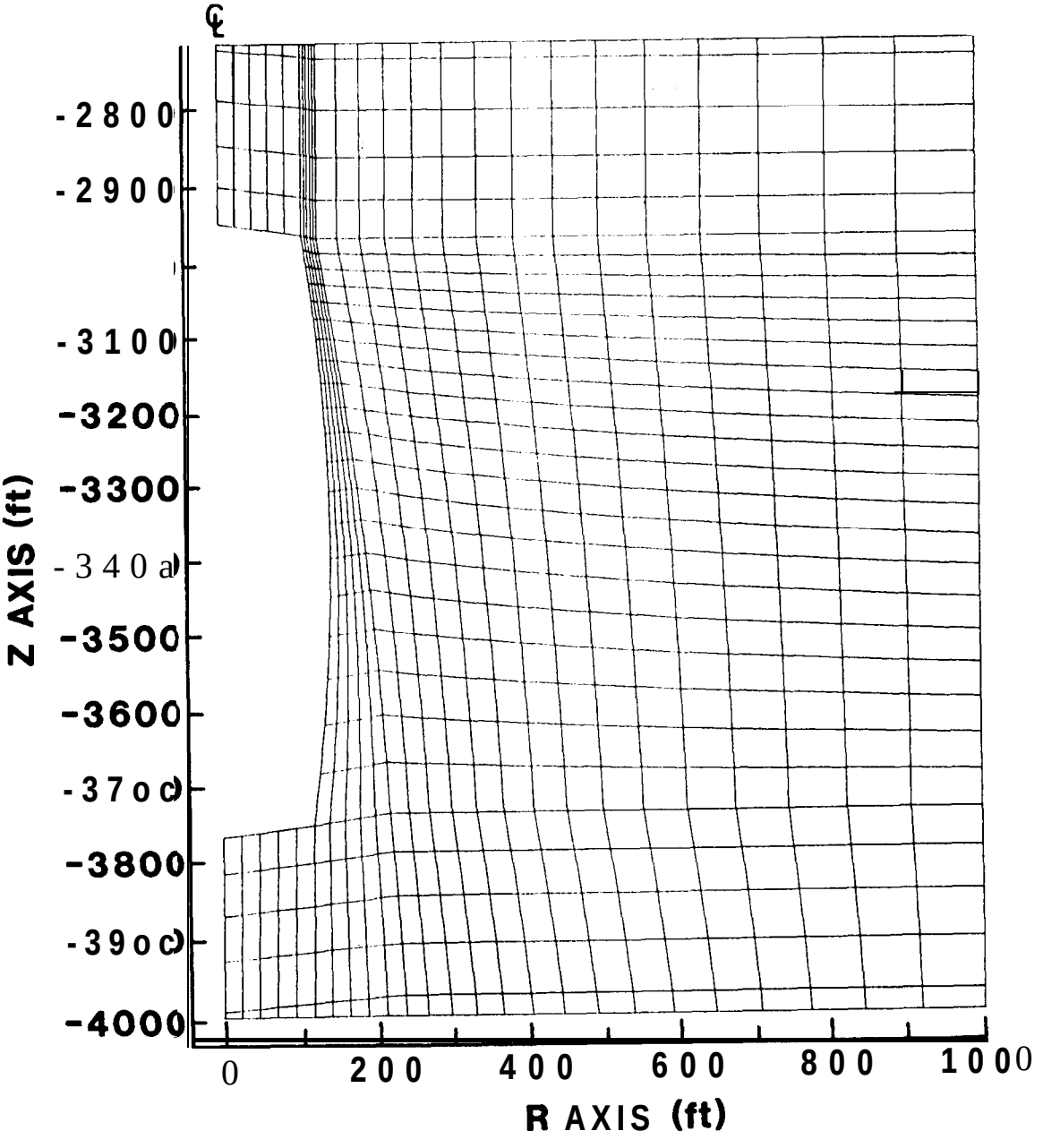

Figure 41. Close-Up of Axisymmetric Finite Element Model of West Hackberry Cavern Eleven.

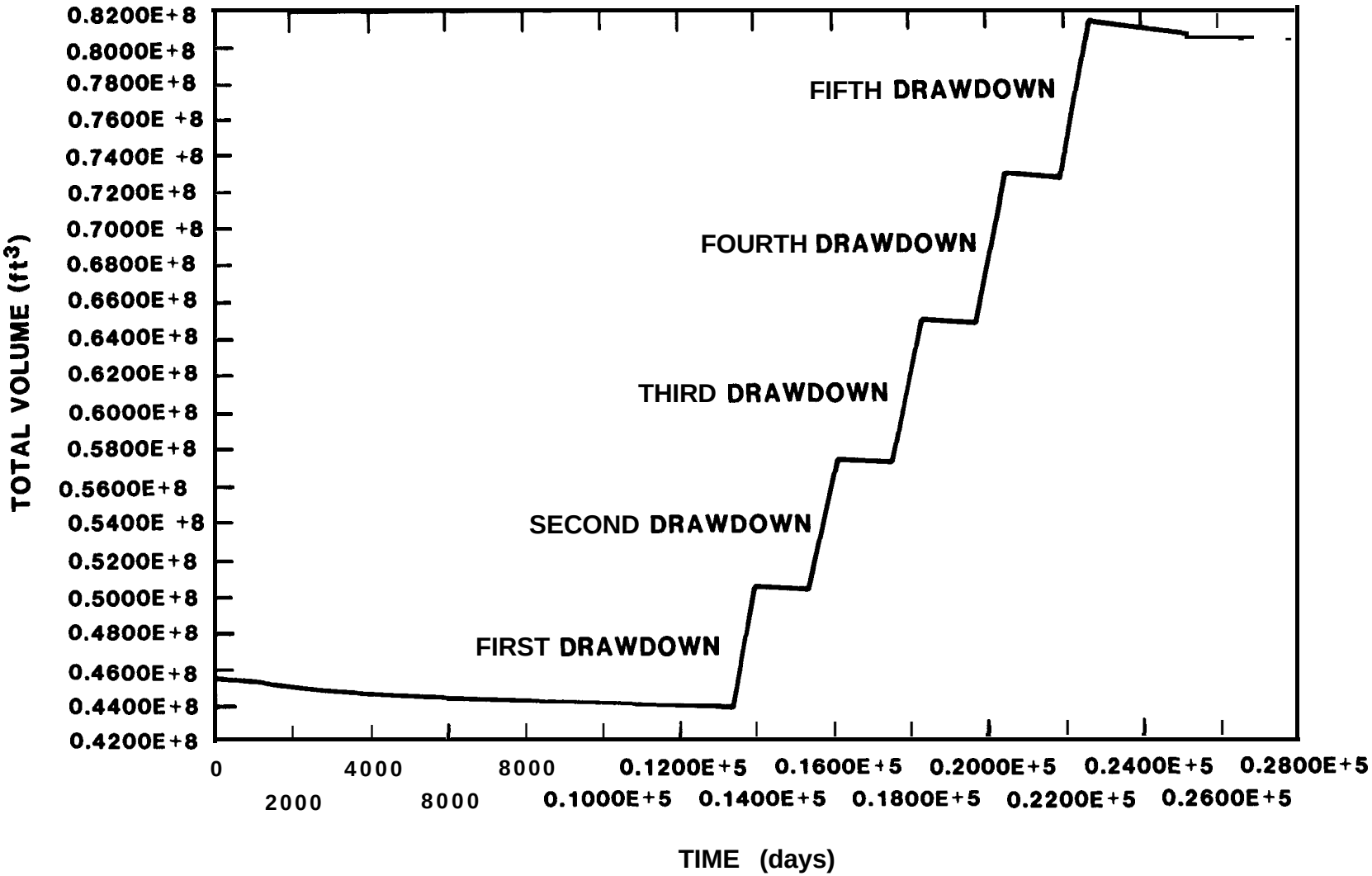

Figure 42. Volumetric Response of West Hackberry Cavern Eleven.

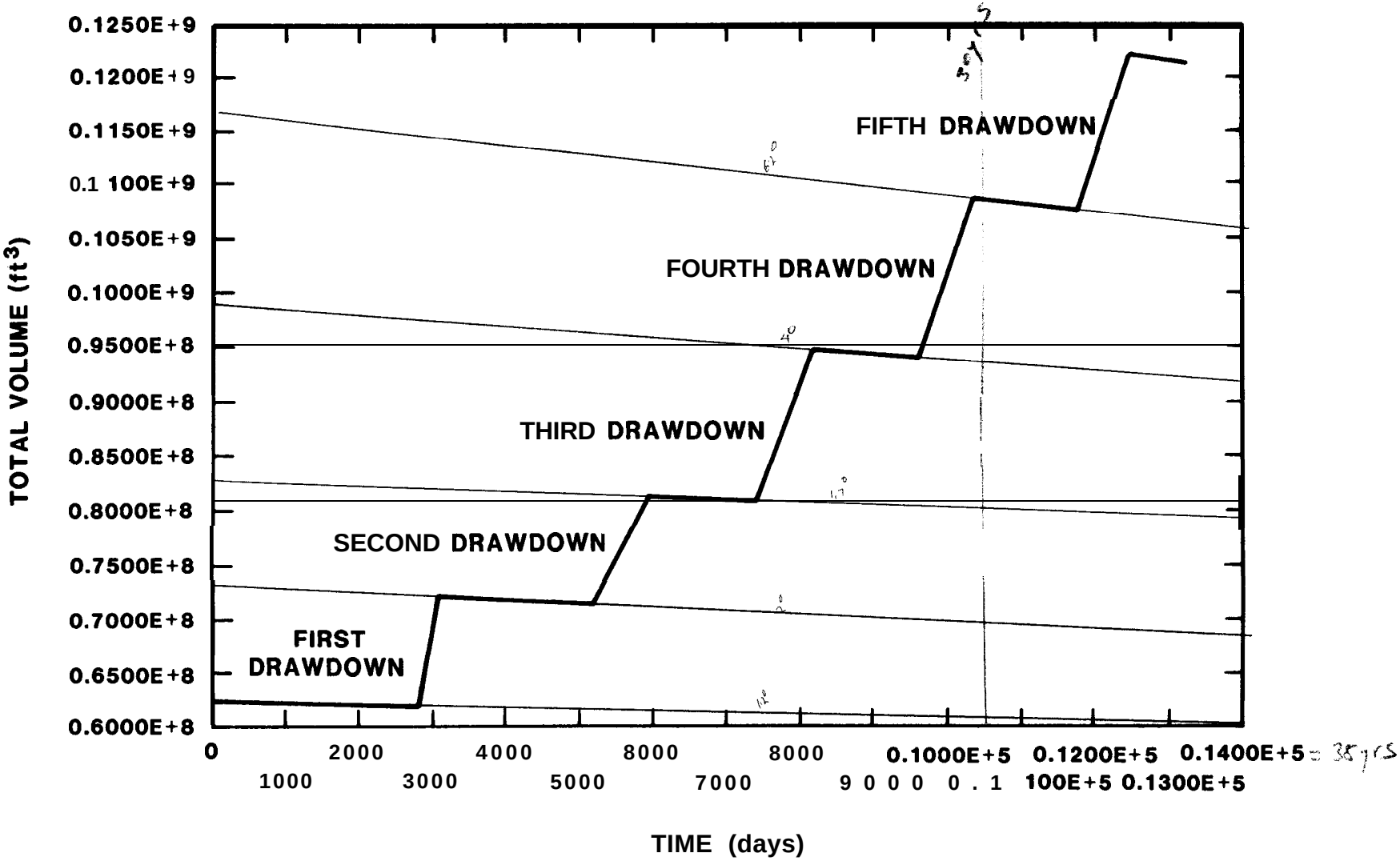

Figure 43. Volumetric Response of West Hackberry Expansion Caverns.

Distribution:

US DOE SPR PMO (8)
900 Commerce Road East
New Orleans, LA 70123
Attn: E. E. Chapple, PMO-581 (6)
TDCS, L. Smith (2)

US Department of Energy (2)
Strategic Petroleum Reserve
1000 Independence Avenue, SW
Washington, DC 20585
Attn: Dave Johnson
Dick Smith

US DOE (1)
Oak Ridge Operations Office
P.O. Box E
Oak Ridge, TN 37831
Attn: P. Brewington, Jr.

Aerospace Corporation (2)
800 Commerce Road East, Suite 300
New Orleans, LA 70123
Attn: K. Henrie
R. Merkle

Walk-Haydel & Associates
600 Carondelet
New Orleans, LA 70112
Attn: R. Haney

POSSI (2)
850 S. Clearview Pkwy.
New Orleans, LA 70123
Attn: K. Mills

1510	J. W. Nunziato
1512	J. C. Cummings
1512	A. J. Russo
1520	D. J. McCloskey
1521	R. D. Krieg
1521	D. S. Preece (30)
1522	R. C. Reuter
1522	J. T. Foley (10)
1530	L. W. Davison
1540	W. C. Luth
1542	B. M. Butcher
1542	W. R. Wawersik
1821	N. E. Brown
3141	C. Ostrander (5)
3144	W. R. Roose (5)
3151	W. L. Garner (3)
3154-3	C. H. Dalin (25)
	DOE/TIC (Unlimited Release)
6200	V. L. Dugan
6250	B. W. Marshall
6257	J. K. Linn (10)
6257	R. R. Beasley
6257	J. L. Todd
6330	W. D. Weart
8424	M. A. Pound

☆ U.S. GOVERNMENT PRINTING OFFICE: 1984-576-I 17110.013